OBSERVATION AND VALIDATION OF NO AND NO_2 FROM FTIR OVER ADDIS ABABA

By

FRIEWELEGA GELETA HUNDE

SUBMITTED IN PARTIAL FULFILLMENT OF THE
REQUIREMENTS FOR THE DEGREE OF
MASTER OF SCIENCE IN PHYSICS
AT
ADDIS ABABA UNIVERSITY
ADDIS ABABA, ETHIOPIA
JUNE 2011

ADDIS ABABA UNIVERSITY

DEPARTMENT OF

PHYSICS

Supervisor: _____

Dr.GIZAW MENGISTU

Examiners: _____

Dr.ELIAS LEWI

_____

Prof. A.V. GHOLAP

ADDIS ABABA UNIVERSITY

Date: **June 2011**

Author: **FRIEWELEGA GELETA HUNDE**

Title: **OBSERVATION AND VALIDATION OF NO and NO_2 FROM FTIR OVER ADDIS ABABA**

Department: **Physics**

Degree: **M.Sc.** Convocation: **JUNE** Year: **2011**

Permission is here with granted to Addis Ababa University to circulate and to have copied for non-commercial purposes, at its discretion, the above title upon the request of individuals or institutions.

Signature of Author

To my father

Geleta Hunde

Table of Contents

List of Tables

List of Figures

Acronyms

AAU Addis Ababa University

AC Alternating Current

ACR Automatic Component Recognition

ADS Analog-to-Digital Conversion

ALFIP Automatic Line FInding Program

CCD Charge Coupled Device

DC Direct Current

DOFs Degree Of Freedom-signal

DTGS Deuterated TriGlycine Sulfate

FFT Fast Fourier Transform

FOV Field Of View

FT Fourier Transform

FTIR Fourier Transform InfraRed

FTS Fourier Transform Spectroscopy

FWHM Full Width at Half Maximum

GMT Greenwich Merdian Time

HITRAN HIgh resolution TRANsmission

IDACC International Detection of Atmospheric Composition and Change

ILS Instrumental Line Shape

InAs Indium Antimonide

INTDIF INTerfering gases based on DIFferences

IPCC Intergovernmental Panel on Climate Change

IR InfraRed

KIT Karsruhe Institute of Technology

LOS Line Of Sight

LST Local Standard Time

MCT Mercury Cadmium Telluride

NASA National Aeronautics and Space Administration

NCEP National Centers for Environmental Protection

OEM Optimal Estimation Method

OMIL Ozone Monitoring Instrument Level

OPD Optical Path Difference

OPUS OPtical User Software

OrNi Organic Nitrate

PAN Peroxy Acetyl Nitrate

PC Personal Computer

RTE Radiative Transfer Equation

SNR Signal Noise Ratio

SZA Solar Zeinth Angle

UV Ultra Violet

VIS VISible

VOC Volatile Organic Compound

VMR Volume Mixing Ratio

Abstract

Since May 2009 atmospheric absorption spectra using the sun as the source of radiation have been recorded by a ground-based high spectral resolution FTIR spectrometer (Bruker IFS120 M). The alignment of the instrument and its stability over time is monitored by nearly regular cell (HBr) measurements. The analysis of this cell measurement using LINEFIT (Version 12) software has indicated the performance of the instrument is very good. The data measured from May, 2009 to February, 2011 were analyzed and interpreted. The latest version of PROFFIT (PROFFIT95) was used to retrieve vertical profiles for NO and NO_2 and their column amount from pressure dependent broadened spectra with the help of Tikhonov-Philips regularization method. Finally total mean daily and monthly column amount of NO_2 is validated with OMIL3 satellite data. The NO and NO_2 VMRs observed at Addis site reach values of 9.247 ppbv and 2.76 ppbv respectively. Both gases are highly dependent on day time solar strength. The maximum partial column amount on 30, May 2009 occured in between 22.1-23.436 km for NO_2 in lower stratosphere and 32.366-34.22 km for NO in middle stratosphere. The concentration of NO_x (NO+NO_2) life time highly depends on the solar zeinth angle. Random and systematic error contribution to retrieval were analyzed and the result shows that the total error contribution due to atmospheric and auxiliary parameters is less than 34.54% for NO and 38.62% for NO_2. The validation of NO_2 with that from OMIL3 was complicated by the fact that OMIL3 measurement are taken during the whole day while FTIR measurements are mostly from 9-14 LST. As a result OMILS NO_2 is expected to be higher than FTIR NO_2 which is indeed found to be the case in this work.

Acknowledgements

First, I am deeply indebted to my advisor Dr.Gizaw Mengistu for his invaluable advices, tireless follow up and friendly approach.
I also to thank all my friends in Dubti, Afar and all Atmosphere students in AAU.
Finally, I thank a memorial kid Ruahama and my family CHEWFs, specially my mother Fatuma Seyd, for her patience, love, and support throughout my study.

Introduction

In addition to its main components the earth atmosphere contains atmospheric trace gases at extremely low abundance. The VMR of these gases are also extremely low, but the gases play key roles in various phenomena such as Ozone depletion and global warming. Nitrogen oxides ($NO_x = NO + NO_2$) are main important atmospheric trace gases and have central importance for atmospheric chemistry. They are precursors in determining tropospheric ozone, aerosol nitrate, and the hydroxyl radical (OH) which is the main atmospheric oxidant. About $2/3^{rd}$ of the global source of NO_x is from fossil fuel combustion (IPCC, 2007) and is concentrated in urban areas. The next important source is the Biomass burning in tropical areas.

Measurements and interpretation of atmospheric trace gas composition has significant importance for a better understanding of budgets, sources and sinks of trace gases important for atmospheric chemistry, greenhouse effect and climate change. For the understanding of physical and chemical states of the stratosphere and upper troposphere and for assessing the impact of stratospheric changes on the underlying troposphere and on global climate, remote sensing observations play an important role. Aiming for high accuracy and precision, the improvement of retrieval strategies and validation by ground-based remote sensing observations is required. Ground-based FTIR solar absorption spectrometry is a well- established remote sensing technique for the measurement of atmospheric trace gases. For many important trace gases ground-based solar absorption FTIR spectrometry is the only remote sensing technique suitable for

the validation of satellites. This thesis has eight chapter.

The theoretical back ground of our atmospheric quantity, concentration and its layer is given in the first chapter; the second chapter discuss about the sources and sinks of nitrogen oxides, its background concentration and atmospheric chemistry in troposphere and stratosphere. The third chapter covers radiative transfer of startified atmosphere. The fourth chapter discusses the principles of remote sensing measument and retrival method.

The FTIR spectrometer setup in our measument site is elaborated in chapter 5. Chapter 6 explains the working principles of FTIR spectroscopy. The ground-based measurement of NO_x over Addis Ababa using FTIR spectrometer and the validation of NO_2 are dicussed in chapter 7 and finally conclusion is presented in Chapter 8.

Chapter 1

The Atmosphere

The Earths atmosphere is a natural laboratory, in which a wide variety of physical processes takes place. It consists of a mixture of ideal gases: although molecular nitrogen and molecular oxygen predominate by volume, the minor constituents carbon dioxide, water vapour and ozone play crucial roles. The forcing of the atmosphere is primarily from the Sun, though interactions with the land and the ocean are also important.

The atmosphere is continually bombarded by solar photons at infra-red, visible and ultra -violet wavelengths. Some solar photons are scattered back to space by atmosphericgases or reflected back to space by clouds or the Earths surface; some are absorbed by atmospheric molecules or clouds, leading to heating of parts of the atmosphere; and some reach the Earths surface and heat it. Atmospheric gases, clouds and the Earths surface emit and absorb infra- red photons, leading to further heat transfer between one region and another, or loss of heat to space.

To determine the atmospheric composition, consider a small sample of air of volume V, temperature T and pressure p, containing a mixture of gases Gs_i(i= 1,2,..). If there are n_i molecules of gas Gs_i in the sample, then [1]

$$n = \sum n_i \tag{1.0.1}$$

where the sum is taken over all the gases in the mixture, and the total mass of the sample is

$$m = \sum m_i n_i \tag{1.0.2}$$

where m_i is the molecular mass of gas Gs_i.

We define the **mass mixing ratio** $[\mu_i]$ of gas Gs_i as the total mass of the molecules of gas Gs_i in the sample, divided by the total mass of the complete sample. Thus

$$\mu_i = \frac{m_i n_i}{m} \tag{1.0.3}$$

The partial pressure p_i of gas Gs_i is the pressure that would be exerted by the molecules of Gs_i from the sample if they alone were to occupy volume 'V' at temperature 'T'; from ideal gas law $pV = nk_BT$, since $k_B = R/N_A$ is Boltzmanns constant (1.381×10^{23} $\mathrm{JK}^{-1}mol^{-1}$) and N_A=6.022×10^{23} mol^{-1} is avogadro number:

$$p_i = n_i \frac{k_B T}{V} \tag{1.0.4}$$

Similarly, the partial volume V_i of gas Gs_i is the volume that would be occupied by the molecules of gas Gs_i from the sample if they, alone, were to be held at temperature 'T' and pressure 'p':

$$V_i = n_i \frac{k_B T}{p} \tag{1.0.5}$$

Dalton's laws of partial pressure $p = \sum p_i$ and partial Volume $V = \sum V_i$, follow immediately from these definitions and Eqn(1.0.1). From Eqns(1.0.3)-(1.0.4) we can relate the mass mixing ratio to the partial pressure as follows:

$$\mu_i = \frac{n m_i p_i}{m p} = \frac{m_i}{\bar{m}} \frac{p_i}{p} \tag{1.0.6}$$

where $\bar{m} = m/n$ is the mean molecular mass for the sample.

We also define the **volume mixing ratio** $[\xi_i]$ (also known as the mole fraction)

$$\xi_i = \frac{V_i}{V} \tag{1.0.7}$$

by Eqns(1.0.5)-(1.0.7) we have

$$\xi_i = \frac{n_i}{n} = \frac{p_i}{p} \tag{1.0.8}$$

Note that the two mixing ratios are related by

$$\mu_i = \frac{n_i}{n}\xi_i \tag{1.0.9}$$

The most commonly used units in mixing ratio for the gas phase species is parts per million (ppm), parts per billion (ppb) and parts per trillion (ppt) of volume [1].

Number density $[n_i]$

It is the ratio of number molecule of species 'i' to the volume of air [molecules per cm^3]. The degree of absorption or scattering depends on the number of molecules of gas along the path of light beam in column of atmosphere. The number density of air in our atmosphere from the sea level (z=0) up to a certain altitude ($z = z_T$) on top layer that the n_k is negligible gives the atmospheric column amount (clmn) of a gas, mathematically

$$clmn = \int_0^{z_T} n_i dz \tag{1.0.10}$$

The number density and the mixing ratio ξ_i of a gas related by the number density of air n_{air}:

$$n_i = \xi_i n_{air} \tag{1.0.11}$$

the number density of air molecules as a function of altitude is given by

$$n_{air}(z) = n_{air}(0)e^{-z/H} \tag{1.0.12}$$

where H is the scale height, $n_{air}(0)$ is the number density at the surface. When we consider for average scale height of 7.4 km and mean surface temperature $288K$ then $n_{air}(0)$=2.55 $\times 10^{19}$ molecules cm^{-3} [2].

1.1 Compositions of the atmosphere

The gaseous envelop that surrounds the earth is known as its Atmosphere. It is a relatively stable mixture of several types of gases from different origins. It has a mass of about 5.15×10^{18} kg held by the gravitational attraction of the planet, the mean molecular mass of air is 28.966 gmol $^{-1}$.

The atmosphere is a mixture of gases, some with fairly constant concentrations, others that are variable in space and time. In addition, there are suspended particles (e.g.aerosol, smoke, ash, etc.) and hydrometeors (e.g.cloud droplets, raindrops, snow, ice crystals, etc.). **Table 1.1** shows the composition of dry air in the Earths atmosphere below 100 km [3].

Table 1.1: Major constituents of the Earths atmosphere upto 100 km (dry air).

Constituents	% by volume	Mole. weight ($gmol^{-1}$)
A]Constant concentrations		
Nitrogen(N_2)	78.08	28.01
Oxygen (O_2)	20.95	32.00
Argon (Ar)	0.933	39.95
Carbon dioxide(CO_2)	0.033	44.01
Neon (Ne)	18.2×10^{-4}	20.18
Helium (He)	5.2×10^{-4}	04.02
Krypton (Kr)	1.1×10^{-4}	83.80
Xenon (Xe)	0.089×10^{-4}	131.29
Hydrogen (H)	0.5×10^{-4}	02.02
Methane (CH_4)	1.5×10^{-4}	16.04
Nitrous oxide(N_2O)	0.27×10^{-4}	44.01
Carbon monoxide (CO)	0.19×10^{-4}	28.01
B]Variable concentrations		
Water vapor (H_2O)	$0 - 4$	18.02
Ozone (O_3)	$0 - 4 \times 10^{-4}$	48.02
Ammonia (NH_4)	0.004×10^{-4}	17.02
Sulphur dioxide (SO_2)	0.001×10^{-4}	64.06
Nitrogen dioxide (NO_2)	0.001×10^{-4}	46.05
Other gases	Trace amounts	–
Aerosol, dust, gases	Highly variable	–

Nitrogen, oxygen, and argon account for about 99.96% of the permanent gases. Of the variable constituents, carbon dioxide can be somewhat variable in concentration on a localized basis at low levels. Water vapor is a highly variable constituent, with concentrations ranging from nearly zero in the coldest and dry regions of the atmosphere up to as much as 4% by volume in hot and humid air masses. Ozone, the other major greenhouse gas, also varies distinctly. In addition to these variable constituents there are also aerosols and hydrometeors which can vary widely in space and time.

More than 99.9% of the total atmospheric mass is concentrated in the first 50 km from Earths surface. At the sea level nitrogen and oxygen make up 99% of the atmosphere with the remainder comprising CO_2, noble gases and traces of many gaseous substances. There is increasing evidence that the percentages of trace gases are changing because of both natural and human (Anthropogenic) factor. CO_2, N_2O, and CH_4 are produced by the burning of fossil fuels, expelled from living and dead biomass, and released by the metabolic processes of microorganisms in the soil, wetlands, and oceans. Atmospheric temperature and chemistry are generally influenced by the trace gases.

Some of the gases do not have uniform mixing ratios (e.g.ozone, water vapour, etc.) in the lowest 100 km. They can have a source at the surface or in the atmosphere, or a sink at the surface or in the atmosphere. If the gas's lifetime is shorter than the time it takes to get transported from one place to another, then the gas may not be uniformly distributed throughout the atmosphere.

Above 100 km, the mixing of air parcels is dominated by molecular diffusion. This part of the atmosphere is subjected to bombardment by radiation and high energy particles from the Sun and outer space [3].

1.2 Vertical Structure of Pressure and Density

The vertical structure of the atmosphere depend on the vertical column of air. Meteorological parameters, such as pressure and air density vary dramatically with height in the atmosphere. The air pressure varies spatially and temporally because the amount and weight of air above the Earth vary with location and time. If vertical accelerations are ignored, Newton's second law of motion applied to the vertical column of air with unit horizontal cross-sectional area in Fig. 1.1. The mass of air $'m'$ between heights z and $z + \delta z$ in the column is $-\rho\delta z$ where ρ is the density of the air at height z. The downward force acting on this slab of air due to the weight of the air is $g\rho\delta z$, where g is the acceleration due to gravity at height z. The net vertical force that acts on the slab of air between z and $z + \delta z$ due to the pressure of the surrounding air. Let the change in pressure in going from height z to height $z+\delta z$ be δp as indicated in Fig. 1.1. Because we know that pressure decreases with height δp must be a negative quantity, and the upward pressure on the lower face of the shaded block must be slightly greater than the downward pressure on the upper face of the block:

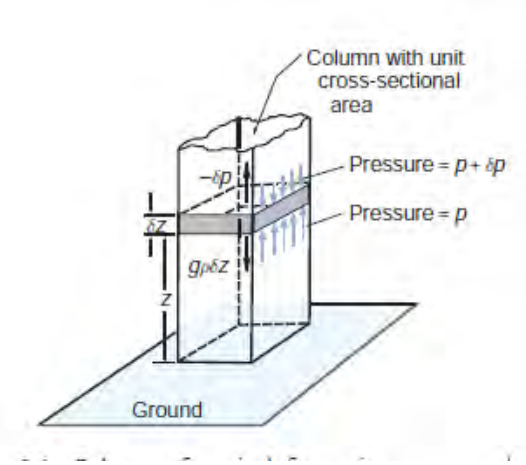

Figure 1.1: Vertical column of air mass density ρ, in the cross sectional area δA, height δz

$$p - (p + \delta p) = -\delta p = g\rho\delta z \tag{1.2.1}$$

and in the limit as $\delta z \rightarrow 0$

$$\frac{dp(z)}{dz} = -\rho g \tag{1.2.2}$$

Since $\rho = \frac{m}{V}$ and $n = \frac{m}{M_{air}}$, 'M_{air}' the average molecular weight of air:

$$\rho(z) = \frac{p(z)M_{air}}{T(z)R} \tag{1.2.3}$$

$$\frac{dp(z)}{dz} = -\frac{p(z)M_{air}}{T(z)R}g \tag{1.2.4}$$

$$\int_{p_0}^{p(z)} \frac{dp(z)}{p(z)} = -\int_0^z \frac{dz}{H(z)} \tag{1.2.5}$$

$$H(z) = \frac{M_{air}\ g}{T(z)R}$$

Since the temperature is approximately constant, then the pressure decrease with height approximately exponetial

$$\frac{p(z)}{p(0)} = e^{-z/H} \tag{1.2.6}$$

If the temperature is not constant (non-isothermal atmosphere), first we define a local scale height: $H(z)$. Therefore the above Eqn (1.2.5) becomes

$$p(z) = p(0)e^{-\int_0^z \frac{dz'}{H(z')}} \tag{1.2.7}$$

From Eqn(1.2.3) and Eqns(1.2.6-1.2.7) we get air mass density of the atmosphere [2].

1.3 Thermal Structure

The layers of the earth atmosphere are characterized by variation in temprature which produce differences in the radiative and chemical composition of the atmosphere at different altitudes. Based on the temprature changes with height, the earth atmosphere is divided into four concentric spherical strata with narrow transition zones as in the **Fig. 1.2**. The layers are sphere and the transitions are pause [3].

Troposphere is the lowest part of the atmosphere and is closer to the Earth, and extends about 8 km above the poles and 18 km over the equator. It is the densest part of the atmosphere which contains almost all the water vapor, clouds and precipitation. Temperature generally decreases with height in the troposphere at about 6-7^{0}Ckm^{-1} in the lower half and 7-8^{0}Ckm^{-1} in the upper half. Because of the general decrease of temperature with height and the presence of weather systems, the troposphere is often characterized by fairly significant localized vertical motions, although these are generally much smaller than horizontal motions. Sometimes shallow layers may be present in the troposphere in which temperature increases with height. These inversions inhibit vertical motion. The presence of water vapor, clouds, storms, and weather contributes to the significance of the troposphere. The troposphere is bounded at the top by the tropopause, whose altitude varies considerably depending on the location and type of weather systems, latitude, etc. This tropopause may be considered as the base of a large inversion layer, i.e. the stratosphere which inhibits vertical mixing. Consequently there are often significant concentration gradients across the tropopause.

Stratosphere is the second major stratum in the atmosphere. It resides above the tropopause upto 50 km. The air temperature in the stratosphere increases gradually to around 273K at the stratopause ($\sim$50 km), which is marked by a reversal in the temperature trend. Because the air temperature in the stratosphere increases with altitude, it does not cause convection and has a stabilizing effect on atmospheric conditions in the region and confines turbulence to the troposphere. As water vapor content with in the stratosphere is very low, ozone plays the major role in regulating the thermal regime of this layer. The stratosphere is a region of intense interactions among radiative, dynamical, and chemical processes, in which horizontal mixing of gaseous components proceeds much more rapidly than vertical mixing. The stratosphere is warmer than the upper troposphere, primarily because of a stratospheric ozone layer that absorbs

solar ultraviolet radiation. The chemical composition of the stratosphere is generally similar to that of the troposphere with some exceptions, the most notable of which are ozone and water vapor. The stratosphere is relatively dry. However, it is rich in ozone as it is the main region of ozone production. Ozone absorbs ultraviolet radiation from the Sun and with the low densities present at stratospheric altitudes, this absorption is an efficient mechanism of transferring kinetic energy to a relatively small number of molecules due to which the air temperature becomes high. Ozone in the upper stratosphere therefore acts as a heat source. Some of the heat is transferred down by subsidence and radiation, although the stratosphere as a whole remains warm at the top, where the temperatures are close to those at the Earths surface, and cold at the bottom and therefore very stable. The level at ($\sim 50 - 55$ km) the temprature ceases to increase with altitude is stratopause.

Mesosphere is a layer extending from 50 to 80 km, is characterized by decreasing temperatures with increasing altitude, reaching about 180K at 80 km. Compared to lower regions, the concentrations of ozone and water vapor in the mesophere are negligible, hence the lower temperatures. Its chemical composition is fairly uniform. Pressures are very low. The mesopause, which separate the mesosphere from the next highest layer and like the other pauses, is a region where the temperature trend changes direction. Like the tropopause, however the temperature of the mesopause can vary quite significantly, dropping as low as 150K so the lowest atmospheric temperatures are usually found.

Thermosphere is a region of high temperatures above the mesosphere. It includes the ionosphere and extends out to several hundred kilometers. The temperatures in this region are of the order of $500 - 2,000K$ and the densities are very low. The increase in temperature in the thermosphere is due to the absorption of intense solar radiation by the limited amount of molecular oxygen present. At an altitude of $100 - 200km$,

the major atmospheric components are still nitrogen and oxygen, although at this high altitude gas molecules are widely separated. The thermopause is the level at which the temperature stops rising with height. Its height depends on the solar activity and is located between 250 and 500 km. Above this the upper boundary region is Exosphere.

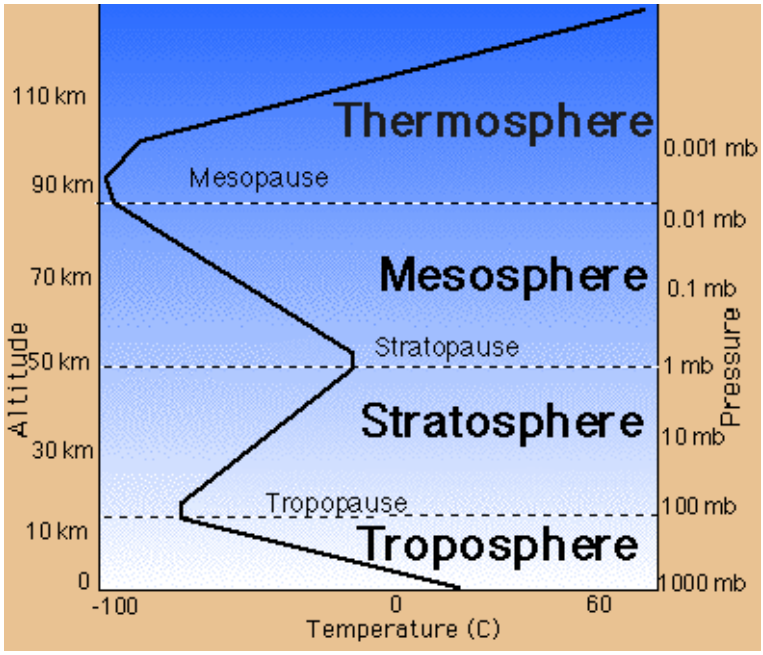

Figure 1.2: Atmospheric layers up to 100km and above.

Chapter 2

Sources & Sinks of Nitrogen Oxides in the Atmosphere

Nitrogen compounds are presents in the atmosphere in both oxidized and reduced forms. The reduced compounds include Ammonia (NH_3) and Ammonium (NH_4). The Oxidized compounds include Nitrous oxide (N_2O), Nitric oxide (NO), Nitrogen dioxide (NO_2), nitrous acid ($HONO$), nitric acid (HNO_3), PAN ($CH_3COO_2NO_2$) and particulate nitrate (NO_3^-). From these, Nitrous oxide (N_2O) is a greenhouse gas and has long residence time and nonreactive behaviour in the troposphere. It is disconnected from the oxidised compounds of nitrogen. The most important atmospheric nitrogen oxides are merged to NO_x. NO_x is a family name; collectively the nitric oxide and nitrogen dioxide ($NO_x = NO + NO_2$). As a whole the reactive oxides refered as NO_y, NO_y is the sum of the two NO_x and all compounds of that are products of the atmospheric oxidation of NO_x [4]:

$$NO_y = NO_x + HNO_3 + PAN + HONO + NO_3^- + N_2O_5 + OrNi, etc \qquad (2.0.1)$$

NO_x, Nitrogen oxides (NO and NO_2) are among the most important molecules in the atmospheric chemistry. It is a primary pollutant that under go several photochemical reactions in sun light forming secondary pollutant species and also a critical component in the photochemistry of the troposphere. NO_x contribute to the formation of acid rain, smog, ozone in the troposphere and destruction of ozone in the stratosphere

and controls the oxidising capacity of troposphere by modifying the supply of a key radical species (OH, RO_2, HO_2). Sources of nitrogen oxides in the atmosphere are anthropogenical (human activity) and natural. The removals from atmosphere by dry deposition as the type of NO_y far from the sources or wet deposition as the type of this by clouds scavenging /wash out by rain/. The life time of NO_x in atmosphere is from hours to a few days.

2.1 Sources of NO_x in the atmosphere

The sources of NO_x in the atmosphere are from human activity (anthropogenical) and also naturally [5]. Natrual processs such as microbial in both soil and water, photochemical destruction of nitrogen compounds from lighting (troposphere) and solar radiance in stratosphere or upper atmosphere, and volcanic activity. Anthropogenical such as combustion of fossil fuel (mobile and stationary sources), biomass burning, aircraft and industrial sources. From these sources the major contribution are combustion fossil fuel and biomass burning from anthropogical; microbial and lighting from natural takes the dominate sources in the atmosphere.

2.1.1 NO_x emissions in the troposphere

In troposphere the release of nitrogen oxides from combustion fossil fuel, biomass burning, lighting and microbacterial process are the significant contributer. But the release of these oxides mainly due to the activity of human has accelerate during the last few decades through primarily in combustion fossil fuel from the northern hemisphere of midlatitude continetal surface and and secondly from biomass burning for the use of land for cultivation in tropical and subtropical regions; it has increased from $5T\mathrm{g}[N]yr^{-1}$, in 1940 to $25T\mathrm{g}[N]yr^{-1}$ in 1995 [6]. In 2001 IPCC estimation of global

NO_x show that the emission increases to $40.1 Tg[N]yr^{-1}$ as the sum of these two human activty [2]. The other best source estimates and emissions location by IPCC(2001) are listed in the Table 2.1. The major contribution comes from combustion of fossil fuels

Table 2.1: Estimate of Global Tropospheric NO_x Emissions in $Tg[N]yr^{-1}$ for Year 2000.

Sources	Emissions ($Tg[N]yr^{-1}$)	Principal location of emissions
Fossil fuel combustion	33.0	Northern hemisphere midlatitude continental surface
Aircraft	0.7	Northern hemisphere, $30 - 60^0 N$
Biomass burning	7.1	Tropical continental surface
Soils	5.6	Non-polar continental surface
NH_3 oxidation	–	Tropical continental surface
Lightning	5.0	Tropical continent troposphere
Stratosphere	< 0.5	Stratosphere
Total	51.9	All above

at high temperature typically with temprature of 2500K [4], NO is produced from the reactions:

$$O_2 \xleftrightarrow{M} 2O \qquad M = N_2, O_2 \tag{2.1.1}$$

$$O + N_2 \xleftrightarrow{M} NO + N \tag{2.1.2}$$

$$\underline{N + O_2 \xleftrightarrow{M} NO + O} \tag{2.1.3}$$

$$NET: \; O_2 + N_2 \longleftrightarrow 2NO \tag{2.1.4}$$

Smaller amounts of NO_2 are released due to the further oxidation of NO, mainly nitrogen present in the fuel and from the oxidation of atmospheric N_2 in the atmosphere presence of O_2. The microbial process in soil of non polar continetal surfaces produces NO_x and N_2O as natural sources with a process of nitrification and denitrification, these depend on soils temprature, soils moisture content and soils vegetation cover. Now a day the use of nitrogenous fertillization for agricultural purpose increases the emission from soils [7]. Lighting emissions occur naturally when thunderstrom

that electrically discharges the air generate NO_x by thermal dissociation of nitrogen molecules due to ohmic heating inside the discharge channel and shock wave heating of the surrounding. Lighting is the dominance source of NO_x in the upper troposphere and also happened in stratosphere, in both sphere [8]. Aircraft is also the source of NO_x in the upper toposphere.

2.1.2 NO_x emissions in the stratosphere

The dominant source of NO_x in stratosphere is the decomposition of N_2O that emit from microbial in the soil. N_2O is unreactive in the troposphere then it enters in the stratosphere. Approximately 90% of N_2O in this process is destroyed by photolysis:

$$N_2O + h\nu \rightarrow N_2 + O(^1D) \tag{2.1.5}$$

The remaining react with $O(^1D)$:

$$N_2O + O(^1D) \rightarrow NO + NO \tag{2.1.6}$$

$$N_2O + O(^1D) \rightarrow N_2 + O_2 \tag{2.1.7}$$

The reaction by Eqn(2.1.6) is the main source of NO_x in the stratosphere. In this sphere nitrogen oxides has the ability to catalytically destuct ozone and interact with the ozone destroying ClO_x and HO_x cycles. Crutzen (1970, 1971) [2], postulated the catalytic destruction of ozone by NO and NO_2 in the middle and upper stratosphere (above 25km) follows the reaction:

$$O_3 + h\nu \rightarrow O(^1D) + O_2 \tag{2.1.8}$$

$$NO + O_3 \xrightarrow{K_1} NO_2 + O_2 \quad ,1^{st} \tag{2.1.9}$$

$$\underline{NO_2 + O(^1D) \xrightarrow{K_2} NO + O_2 \quad ,2^{nd}} \tag{2.1.10}$$

$$NET: \ O_3 + O(^1D) \rightarrow 2O_2 \tag{2.1.11}$$

At the first reaction (Eqn 2.1.9) the characterstic time of NO, $\tau_1 = \frac{1}{K_1[O_3]}$ at 25km (Temp=222K) is $\tau_1 \cong 70s$ and the second reaction (Eqn 2.1.10) characterstic time of NO_2, $\tau_2 = \frac{1}{K_2[O(^1D)]}$ at this height is $\tau_2 \cong 800s$ so the rate of these reaction is controlled by the second.

In competition with the second reaction NO_2 absorbs the radiation then it photolysis to

$$NO_2 + h\nu \rightarrow NO + O \tag{2.1.12}$$

followed by

$$O + O_2 + M \rightarrow O_3 + M \tag{2.1.13}$$

If the first reaction followed by third reaction, then no net O_3 destruction takes place because of the O atom in third reaction (Eqn 2.1.12) rapidly combines with O_2 of the first reaction so it reforms O_3 in fourth reaction (Eqn 2.1.13). But if on other hand the second reaction follows, then the O_3 and O (odd molecules of oxygen) are converted to two O_2 molecules.

In upper stratosphere the concentration of O is high therefore the second reaction is effective [9]. Other than NO_x, there is two cycles that destroy ozone in this sphere such as ClO_x and HO_x cycles. But NO_x molecules are linked to these cycles by offering the pathway for deactivation of radicals through the reaction of

$$NO_2 + ClO + M \rightarrow ClONO_2 + M \tag{2.1.14}$$

$$NO_2 + OH + M \rightarrow HNO_3 + M \tag{2.1.15}$$

This prevents the chlorine deactivation and chlorine cycle from further destroying ozone.

In lower stratosphere NO_x cycles react with ozone and forms nitrate radical, at night

$$NO_2 + O_3 \rightarrow NO_3 + O_2 \tag{2.1.16}$$

during day time this nitrate radical rapidly photolyzes to

$$NO_3 + h\nu \rightarrow NO_2 + O \tag{2.1.17}$$

or

$$NO_3 + h\nu \rightarrow NO + O_2 \tag{2.1.18}$$

Eqn (2.1.17) participate to generate O_3 but Eqn (2.1.18) paticipate in overall loss of odd oxygen.

At night time at levels ranging from less than a few ppt in remote regions to several hundred ppt in polluted atmospheres.

2.2 Sinks of NO_x in the atmosphere

In the **Stratosphere**; the main sink of NO_x is the reaction that is given by Eqn (2.1.15) because it is relatively stable in lower part of stratosphere and can be transported to the troposphere. At night time the OH radical in this reaction is absent and the loss of NO_x takes place throughthe oxidation of NO_2 with ozone and form NO_3 in the reaction of Eqn (2.1.16) but this photolyzes back to NO_2 during day

The reaction

$$NO_3 + NO_2 + M \rightleftarrows N_2O_5 + M \tag{2.2.1}$$

is the only known source of N_2O_5 in the atmosphere, and because NO_3 is only present at significant concentrations at night due to its rapid photolysis, the formation of N_2O_5 is restricted to the dark side of the day. This dinitrogen pentaoxide reacts with water vapour in the gas phase that sinks as nitric acid:

$$N_2O_5 + H_2O \rightleftarrows 2HNO_3 \tag{2.2.2}$$

or else when sun rises, N_2O_5 is photolysed back to NO_2.

In **troposphere**; the removal from the troposphere through conversion to HNO_3,

nitric acid, which readily dissolves in to any available water droplets. The other removal form of NO_x takes place, when it reacts with $(OH, O_3, NO_3, HO_2, RO \text{and} RO_2)$. These reaction, however do not play a significant role for the removals because it decompose back to the reactants. The reaction of NO_2 with RO in the upper troposphere leeds to extension of the life time of NO_2 in order of 2 months, which is too slow to be a significant sinks for NO_2 as a form of PAN. The life time of the other reaction product is smaller than PAN. Most of these molecules decomposes thermally or photolytically after transport upto 200 km from their source. In the neighborhood of industrial or urban sources, there is a distinct diurnal pattern in the concentration of NO_x [10]. However these sinks surve as reserviours for NO_x.

2.3 NO_x and photochemistry in the Troposphere

In the troposphere nitrogen oxides are a significant contributor to poor air quality. Both NO and NO_2 are harmful to lung tissue and, as a powerful oxidizing agent, NO_2 is harmful to biological tissue generally. Besides its direct effects, photolysis of NO_2 contributes to ozone production [9]. The chemistry of remote and polluted regions differs in the concentration NO_x. NO_x in troposphere play key role in the controls of oxidant capacity and also production of ozone. Ozone is mainly formed indirectly by the action of sunlight on nitrogen dioxide as a result of the various reactions that take place in the atmosphere. First the source mostly of NO_x from the surface is NO, which can rapidly react with ozone to create NO_2 by the reaction:

$$NO + O_3 \rightarrow NO_2 + O_2 \tag{2.3.1}$$

So, nitrogen dioxide molecule undergoes photolysis by solar radiation in the near UV and Vissible spectra range λ(300-420nm) with the products of exit oxygen $O(^3P)$ and nitric oxide. But exit atom reacts with molecules of oxygen that again produces ozone.

The dissociation of this nitrogen dioxide is the only gas that absorbs photon in the lower atmosphere:

$$NO_2 + h\nu(300 < \lambda < 420nm) \rightarrow NO + O(^3P) \tag{2.3.2}$$

$$O(^3P) + O_2 + M \rightarrow O_3 + M \tag{2.3.3}$$

All the above three relations make up a null cycle with no net production of ozone [2,4]. Therefore the equillibrium photostationary state happened.

Ozone formation occurs through the following sequences of reactions primarily the reaction of VOC or Carbon monoOxide(CO) with Hydroxyl(OH) then followed by the conversion of NO to NO_2 (NO react with HO_2 or RO_2). The NO_2 undergoes with photolysis to generate atomic oxygen and combine with O_2 to reform O_3 with out destroying ozone molecules [9]:

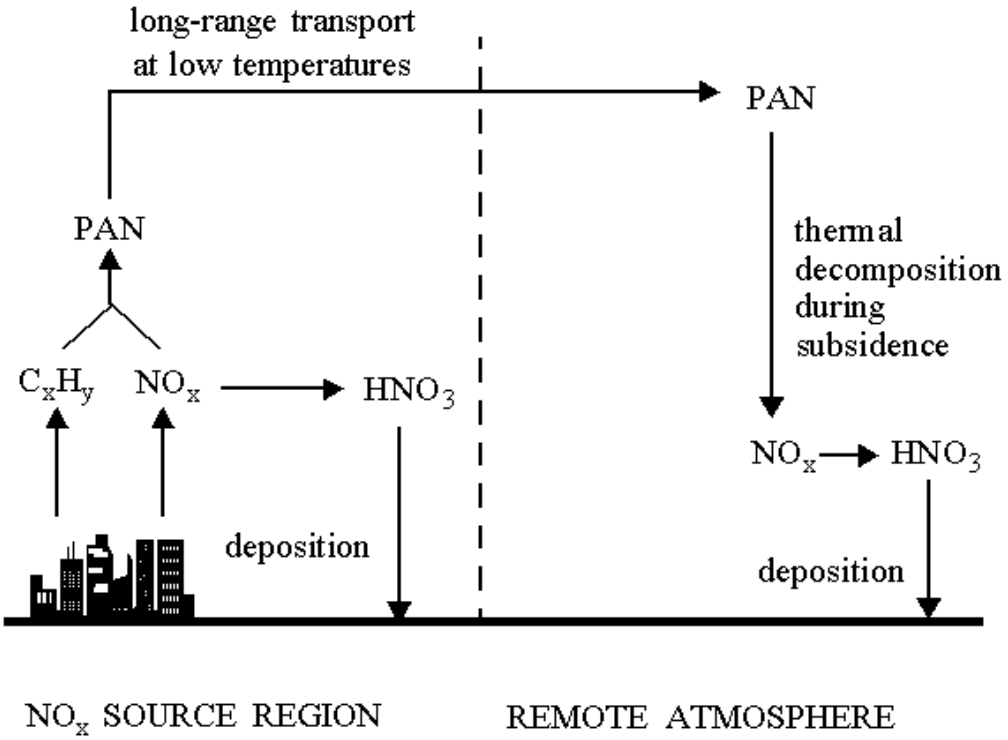

Figure 2.1: Transportation of NO_x from its source to remote area.

$$CO + OH \rightarrow CO_2 + H \tag{2.3.4}$$

$$H + O_2 \rightarrow HO_2 \tag{2.3.5}$$

$$\underline{HO_2 + NO \rightarrow OH + NO_2} \tag{2.3.6}$$

$$NET: \ CO + O_2 + NO \rightarrow CO_2 + NO_2 \tag{2.3.7}$$

which then undergoes

$NO_2 + h\nu \rightarrow NO + O$

$O + O_2 + M \rightarrow O_3 + M$

The NO_x molecules could catalize the ozone production in the polluted boundary layer and under summer time radiative conditions jointly responsible for summer smog episodes. There is also chemistry of NO_x that involves other chemicals as shown in Fig. 2.1. These processes are indeed responsible for long range transport of NO_x.

Chapter 3

Radiative Transfer in the Atmosphere

3.1 Emission and Extinction

Radiation and matter have only two forms of intraction; extinction and emission. The two process are distinguished by a sign of the change of the radiant intensity I_ν as result of interaction. If the intensity decreases the extinction increases the emission [11]. The extinction of radiation first proposed by "LAMBERT", stated that the extinction (i.e reduction) of radiation traversing to an infinitesmal path ds is linearly proportional to the incident radiation and amount of interacting matter along the path:

$$dI_\nu = -k_\nu \rho I_\nu ds \tag{3.1.1}$$

where; ρ- the density of the material, s -the absorber path length, k_ν- the mass extinction cross section for radiation ν. k_ν includes the mass absorption and scattering cross section. Thus the reduction in intensity is due to absorption by the material as well as to scattering by the material, both are removing photons from the beam.
Similarily the radiation's intensity may be strengthened by the emission from the material plus multiple scattering from all other directions into the pencil under consideration at the same wavelength:

$$dI_\nu = j_\nu \rho ds \tag{3.1.2}$$

where j_ν the source function coefficient.

Extinction and emission are linear processes, and thus additive. Since they are only two processes which alter intensity of radiation:

$$dI_\nu = -k_\nu \rho I_\nu ds + j_\nu \rho ds \tag{3.1.3}$$

$$dI_\nu = (-I_\nu + \frac{j_\nu}{k_\nu}) k_\nu \rho ds \tag{3.1.4}$$

After defining $J_\nu = \frac{j_\nu}{k_\nu}$, source function that has units of radiant intensity, we obtain

$$\frac{dI_\nu}{k_\nu \rho ds} = -I_\nu + J_\nu \tag{3.1.5}$$

This is the general RTE.

If the diffuse radiation produced by multiple scattering can be neglected, then Eq. (3.1.5) reduces to the following form:

$$\frac{dI_\nu}{k_\nu \rho ds} = -I_\nu \tag{3.1.6}$$

3.2 Optical Depth

Optical depth (τ) is the vertical component of the optical path, that measures extinction between vertical level. It is a dimensionless parameter which quantifies the attenuation of the sun's light beam [12].

In this path the fraction of incident beam has been attenuated due to absorption and /or scattering. From the above "Beer's" law. we get

$$I_\nu(z) = I_\nu^0 \exp^{-\int (k_\nu \rho)(\sec\theta) dz} \tag{3.2.1}$$

after integration over the path length. Defining $ds = (\sec\theta)dz$, we arrive at

$$\frac{I_\nu(z)}{I_\nu^0} = \exp^{-\tau_\nu \sec\theta} \tag{3.2.2}$$

where $\tau_\nu = \int_z^\infty k_\nu \rho dz$ is optical depth.

We can also define transmitivity by

$$\frac{I_\nu(z)}{I_\nu^0} = T_\nu \tag{3.2.3}$$

$$i.e. \qquad T_\nu = \exp^{-\tau_\nu \sec\theta} \tag{3.2.4}$$

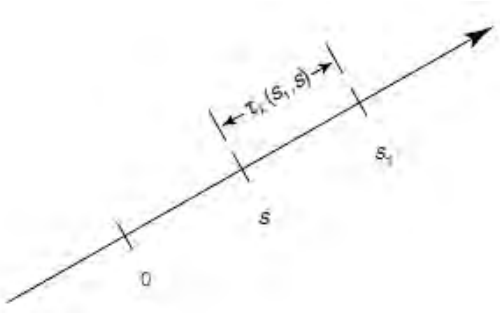

Figure 3.1: Configuration of the optical thickness τ_ν.

For any layers between two points s_1 and s in Fig 3.1, we can evaluate optical thickness as

$$\tau(s_1, s) = \int_{s_1}^{s} k_\nu \rho ds' \tag{3.2.5}$$

or in differential form as

$$d\tau_\nu(s_1, s) = -k_\nu \rho ds \tag{3.2.6}$$

thereby rewriting Eq.(3.1.5) as

$$-\frac{dI_\nu(s)}{d\tau_\nu(s_1, s)} = -I_\nu + B_\nu[T(s)] \tag{3.2.7}$$

where $J_\nu = B_\nu[T(s)]$, the source function.

3.3 Radiative Transfer Equation in Stratified Atmosphere

For many atmospheric radiative transfer applications, it is physically appropriate to consider that the atmosphere in localized portions is plane-parallel such that variations in the intensity and atmospheric parameters (temperature and gaseous profiles) are permitted only in the vertical direction (i.e., height and pressure). In this case, it is convenient to measure linear distances normal to the plane of stratification (see Fig. 3.2). If z denotes this distance, then the general equation of radiative transfer Eqn. 3.1.5 becomes [11]

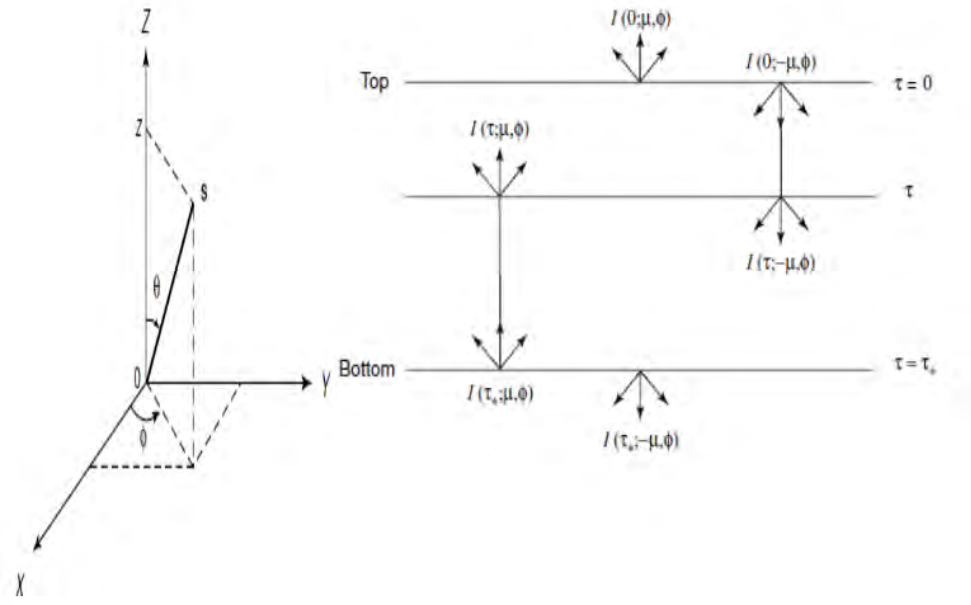

Figure 3.2: Upward (μ) and downward ($-\mu$) intensities at a given level τ and at top ($\tau = 0$) and bottom ($\tau = \tau^*$) levels in a finite, with geometery of plane-parallel atmosphere θ (zeinth), ϕ (azimuthal) angle and s-position vector.

$$cos\theta \frac{dI_\nu(z;\theta,\phi)}{k\rho dz} = -I_\nu(z;\theta,\phi) + J_\nu(z;\theta,\phi) \tag{3.3.1}$$

where θ denotes the inclination to the upward normal, and ϕ the azimuthal angle in reference to the x axis.

Introducing the normal optical thickness (or depth)

$$\tau(z_1; z_2) = \int_z^\infty k_\nu \rho dz' \tag{3.3.2}$$

measured downward from the outer boundary, it becomes $d\tau = -k\rho dz$

$$\mu \frac{dI_\nu(\tau; \theta, \phi)}{d\tau} = I_\nu(\tau; \theta, \phi) - J_\nu(\tau; \theta, \phi) \tag{3.3.3}$$

where $\mu = cos\theta$. This is the basic equation for the problem of multiple scattering in plane-parallel atmospheres.

The upward and downward intensities for a finite atmosphere that is bounded on two sides at $\tau = 0$ and $\tau = \tau_*$ is given in Fig. 3.2.

To obtain the upward intensity ($\mu > 0$) at level τ we multiply by a factor $e^{-\tau/\mu}$ and perform integration from τ to $\tau = \tau_*$

$$I(\tau; \mu, \phi) = I(\tau_*; \mu, \phi) e^{-(\tau_* - \tau)/\mu} + \int_\tau^{\tau_*} J(\tau'; \mu, \phi) e^{-(\tau' - \tau)/\mu} \frac{d\tau'}{\mu} \quad (1 \geq \mu > 0) \tag{3.3.4}$$

To obtain the upward intensity ($\mu < 0$) at level τ we multiply by a factor $e^{\tau/\mu}$ and μ is replaced by $-\mu$. After carrying out integration from $\tau = 0$ to τ, we obtain

$$I(\tau; -\mu, \phi) = I(0; -\mu, \phi) e^{-\tau/\mu} + \int_0^\tau J(\tau'; -\mu, \phi) e^{-(\tau - \tau')/\mu} \frac{d\tau'}{\mu} \quad (1 \geq \mu > 0) \tag{3.3.5}$$

Chapter 4

Principle of Remote sensing and Retrival method

4.1 Principle of Remote Sensing

Remote sensing is the science of acquiring information about the Earth's surface without actually being in contact with it. This is done by sensing and recording reflected or emitted energy and processing, analyzing, and applying that information. In much of remote sensing, the process involves an interaction between incident radiation and the targets of interest [12].

The basic principle associated with remote sensing of atmospheric constituents involves the interpretation of radiometric measurements of electromagnetic radiation in specific spectral intervals which are sensitive to some physical aspects of the medium. The most important process responsible for energy transfer in the atmosphere is electromagnetic radiation.

4.1.1 Atmospheric absorption line positions

The interaction of radiation and matter is discussed Chapter 3, only in two ways (extinction or emission). In the FTIR spectroscopy, we usually consider absorption spectra. The characteristic absorption features are caused by molecules absorbing

radiation at frequencies that correspond to the allowed transitions between different energy levels. The absorption spectrum of a gas consists of a complex array of lines that correspond to transitions between the discrete electronic, vibrational, and rotational energy levels of molecules. The fundamental requirement for infrared activity, leading to absorption of infrared radiation, is that there must be a net change in dipole moment during the vibration for the molecule or the functional group under study. An IR wave is in between microwave and visible spectrum of electromagnetic radiation. We classify this wave in three IR region according to its wave number [13]: Far-infrared, Mid-infrared and Near-infrared.

A molecule absorbs infrared light when the incoming radiation will create a change in electric dipole moment 'M' during the vibration [14]. This is the selection rule for infrared spectroscopy. Diatomic molecules with the same atoms, in principle, can not be excited to vibrate, because they do not have a dipole moment. Nitrogen (N_2), Oxygen (O_2) and Hydrogen (H_2) are examples of these molecules. Because these molecules do not interfere with the infrared spectrum these molecules are ideal as buffer gas.

The relation of energy and electromagnetic radiation is given by

$$E = hc\tilde{\nu} \tag{4.1.1}$$

where the Plancks constant is h ($6.626\times10^{-34}\ Js^{-1}$), wavenumber $\tilde{\nu}$ and the speed of light c through a vacuum ($2.998\times10^{8}\ ms^{-1}$).

A molecule may undergo a transition to a higher energy level by absorbing electromagnetic radiation and it may drop to a lower level by emitting radiation. Absorption and emission can occur only in association with discrete changes in energy level $\Delta E = E' - E''$ [14]. This is given by

$$\tilde{\nu} = \frac{\Delta E}{hc} \tag{4.1.2}$$

Rotational transition

The rotational energy E_r is defined as

$$E_r = \frac{h^2}{8\pi^2 I} J(J+1) \qquad J = 0, 1, 2, .. \tag{4.1.3}$$

where, I is the moment of inertia, and J the rotational quantum number. The term $\frac{h^2}{8\pi^2 c.I} = B$, is known as rotational constant.

Vibrational transition

The vibratonal energy E_v is defined as

$$E_v = h\nu(v + 1/2) \qquad v = 0, 1, 2, ... \tag{4.1.4}$$

and the vibrational term, which indicates the frequency steps between the vibrational quantum numbers:

$$G(v) = \frac{E_v}{hc} = \tilde{\nu}(v + 1/2) \tag{4.1.5}$$

The bonds between the atoms will break when enough energy is supplied to the molecule. Hence the potential energy will not increase to infinity when the vibrational quantum number is increased above a certain limit.

Simultaneously rotation and vibrational transition

Of course, rotation and vibration of molecules happens simultaneously. The interatomic distance, depends not only on the centrifugal forces of rotation but also on the vibrational state. These vibrational and rotational interactions increase the moment of inertia. The actual rotational constant B_v is smaller than the rotational constant B from Eqn. (4.1.3):

$$B(v) = B - \alpha(v + 1/2) \tag{4.1.6}$$

where α is a constant smaller than B.

Finally the wavenumber of the absorbed radiation results from

$$\tilde{\nu} = G(v') - G(v'') + B'_v J'(J'+1) - B''_v J''(J''+1) \tag{4.1.7}$$

where $G(v') - G(v'')$ is the vibrational transition and $B'_v J'(J'+1) - B''_v J''(J''+1)$ is the rotational transition.

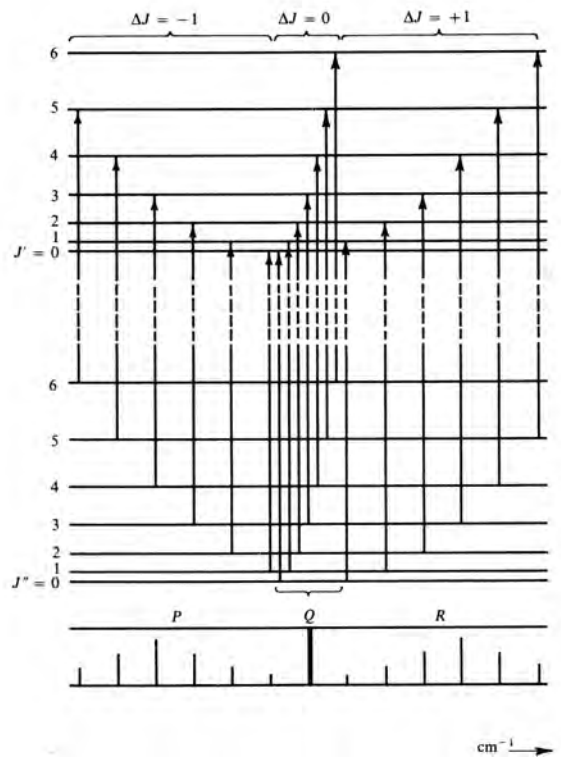

Figure 4.1: Term scheme of rotational and vibrational transition.

Fig. 4.1 give the term schematic of rotational and vibrational transitions. For $\Delta J = +1$ the R-branch is given and for $\Delta J = -1$ the P-branch is given. When $\Delta J = 0$ there is pure vibrational transition. This branch is called the Q-branch. For the Q-branch all the spectral lines are grouped, which results in an intense absorbance line.

Normal modes of vibration

Diatomic molecules can only have one vibrational degree of freedom. Multi-atomic molecules can have more possible number of vibrational modes. The molecules will have 3N degrees of freedom in total. In three of these the atoms move in the same direction, thereby the center of the mass will change in the same position. These motions are called the translation motions. For linear molecules there are two rotational

motions and non-linear molecules have three rotational motions.The number of vibrational modes is given by $Z_{non-linear} = 3N - 6$, For non-linear molecules with N, the number of atoms. And for linear $Z_{linear} = 3N - 5$ [15].

4.1.2 Line broadening and line shapes

As a consequence of Heisenbergs uncertainty principle, absorption lines are never infinitely narrow [14]. The uncertainty in the energy of a state multiplied by the uncertainty in time (the lifetime of a state) must be greater or equal to $\hbar$, ($\Delta E \Delta t \geq \hbar$). So the shorter lifetime, the larger the uncertainty in a state energy and the broader the absorption or emission line (as the energy uncertainty manifests itself as an uncertainty in the frequency of the line). Uncertainty broadening due to the radiative or intra-molecular lifetime of the state in isolation is always present but for vibrational-rotational states is usually very small ($< 10^{-6} cm^{-1}$).

Another form of uncertainty broadening, which dominates at atmospheric pressures, is collisional broadening (also called pressure broadening) and occurs when the collisions of atoms, ions or gas molecules shorten the lifetime of states [14]. In gases it is proportional to pressure and this means that absorption lines from spectra taken through the whole atmosphere will have different shapes depending upon the distribution of the absorbing gas in the atmosphere. A gas that is mainly located in the troposphere will display broad absorption lines because of the high pressure whilst predominantly stratospheric gases will produce much narrower lines since the pressure is low. Uncertainty broadening leads to a Lorentzian line shape contribution at a given wavenumber $\tilde{\nu}$

$$f_L(\tilde{\nu}) = \frac{\alpha_L}{\pi[(\tilde{\nu} - \tilde{\nu}_0)^2 + \alpha_L^2]} \tag{4.1.8}$$

where $\tilde{\nu}_0$ is the absorption line frequency in wavenumbers, and α_L is the Lorentzian half-width at half height, which is proportional to the total pressure.

Absorption lines due to atmospheric gases are also subject to Doppler broadening. Doppler broadening occurs because molecules that travel with different velocities with respect to the light source, absorb at different wavelengths, just as light from stars accelerating away from the Earth is red-shifted. Doppler broadening produces a Gaussian line shape due to the Gaussian distribution of molecular velocities [14]:

$$f_D(\tilde{\nu}) = \frac{1}{\alpha_D\sqrt{\pi}}\exp\left[-(\frac{\tilde{\nu}-\tilde{\nu}_0}{\alpha_D})^2\right] \tag{4.1.9}$$

where $\alpha_D = \frac{\tilde{\nu}_0}{c}\sqrt{\frac{2K_BT}{m}}$ is the Gaussian half-width at half height and m is the mass of the molecule. In this expression of half- width of the line (i.e., the distance between the center of the line and the points at which the amplitude is equal to half the peak amplitude) is $\alpha_D\sqrt{\ln 2}$.

Pressure broadening (with Lorentzian lineshape) dominates in the troposphere, but its effects drop off rapidly with altitude as the pressure drops. Doppler broadening (with Gausssian line shape) is temperature dependent but its variation through the atmosphere is much smaller than pressure broadening. Stratospheric gas lines are primarily Doppler broadened and the two types of broadening become equally significant at around 25Km. The convolution of Lorentzian and Gaussian line shapes produces a Voigt line shape. This variation of the shape and width of absorption lines with the pressure of the absorbing gas means that spectra of atmospheric gases contain information about the altitude of the absorbing gas as well as the total number of absorbing molecules in the path.

The absorption spectra in the vicinity of pressure- and Doppler-broadened absorption lines can be represented by

$$k_{\tilde{\nu}} = Sf(\tilde{\nu}-\tilde{\nu}_0) \tag{4.1.10}$$

where S-is the line intensity/line strength

$$S = \int_0^\infty k_{\tilde{\nu}}d\tilde{\nu} \tag{4.1.11}$$

$\tilde{\nu}_0$-the wavenumber on which the line is centered, and f the so-called shape factor or line profile.

The line intensity for a transition of a molecule with permanent dipole moment of $M(m_i, n_j)$ from the energy level of E_m to E_n with m and n molecules per unit volume [15] is

$$S = \frac{2\pi^2\tilde{\nu}}{3h\varepsilon_0 c}(\frac{N_m}{g_m} - \frac{N_n}{g_n})\sum_{i,j}|M(m_i, n_j)|^2 \tag{4.1.12}$$

where g_m and g_n are the total degeneracy of the states at energy levels of E_m and E_n respectively and 'i' and 'j' represent the i^{th} and j^{th} energy levels of the degenerate E_m and E_n energy states. The line strength can also be expressed precisely in terms of the absorption coefficient of a molecule with these energy levels '$k_{m,n}$'

$$k_{m,n} = \frac{8\pi^2 n g_n}{3hcQ}\tilde{\nu}_{m,n}|M(m_i, n_j)|^2(e^{-\frac{E_m}{K_B}T} - e^{-\frac{E_n}{K_B}T}) \tag{4.1.13}$$

where Q is the total internal partition function.

4.2 Retrival Method

There are several methods of mathematical calculation in the retrival method; in this paper we used the Rogers Optimal Estimation method [19]. The OEM is commonly employed in the underdetermined problem of deriving a vertical profile of an atmospheric trace gas from a ground-based solar absorption spectrum. In OEM the a priori knowledge, $\mathbf{x_a}$, of the n-dimensional state vector $\mathbf{x}$ (e.g., the vertical profile of the trace gas of interest) is combined with the m-dimensional measurement vector $\mathbf{y}$ (e.g., spectral measurements related to the vertical profile by a nonlinear forward model) as a weighted mean. The weights are determined by the (matrix) covariance of the a priori profile, $\mathbf{S_a}$ and the (matrix) covariance of the random spectral measurement noise ϵ, given by $\mathbf{S}_\epsilon$. If the forward model $\mathbf{F}$, including model parameters $\mathbf{b}$ such as pressure,

atmospheric profile, is linear in $\mathbf{x}$, i.e.

$$\mathbf{y} = \mathbf{F}(\mathbf{x}, \mathbf{b}) + \epsilon = \mathbf{K}\mathbf{x} + \epsilon \tag{4.2.1}$$

where $\mathbf{K_{i,j}} = \frac{\partial \mathbf{F_i(x)}}{\partial \mathbf{x_j}}$ is the Jacobian matrix (or weighting function). The optimal solution is given by

$$\hat{\mathbf{x}} = (\mathbf{K^T S_\epsilon^{-1} K} + \mathbf{S_a^{-1}})^{-1}(\mathbf{K^T S_\epsilon^{-1} y} + \mathbf{S_a^{-1} x_a}) \tag{4.2.2}$$

$$\hat{\mathbf{S}} = (\mathbf{K^T S_\epsilon^{-1} K} + \mathbf{S_a^{-1}})^{-1} \tag{4.2.3}$$

where $\hat{\mathbf{S}}$ is a covariance matrix. The linear combination of two scalars with known variances, can also be written as

$$\hat{\mathbf{x}} = \mathbf{x_a} + \mathbf{G}[\mathbf{K}(\mathbf{x} - \mathbf{x_a}) + \epsilon] = \mathbf{x_a} + \mathbf{A}(\mathbf{x} - \mathbf{x_a}) + \mathbf{G}\epsilon \tag{4.2.4}$$

where the gain matrix G is given by

$$\mathbf{G} = (\mathbf{K^T S_\epsilon^{-1} K} + \mathbf{S_a^{-1}})^{-1}\mathbf{K^T S_\epsilon^{-1}} \tag{4.2.5}$$

and the averaging kernel matrix or resoliving kernel $\mathbf{A} = \mathbf{GK}$. The rows of the $n \times m$ $\mathbf{G}$ matrix are commonly referred to as the contribution functions and represent the sensitivity of the retrieved state to the measurements. The rows of the $m \times n$ $\mathbf{K}$ matrix are commonly referred to as weighting functions and represent the sensitivity of the forward model to the true state. By definition, the rows of the $n \times n$ $\mathbf{A}$ matrix give the sensitivity of the retrieved state to the true state:

$$\mathbf{A} = \mathbf{GK} = \frac{\partial \hat{\mathbf{x}}}{\partial \mathbf{y}} \frac{\partial \mathbf{F}(\mathbf{x})}{\partial \mathbf{x}} = \frac{\partial \hat{\mathbf{x}}}{\partial \mathbf{x}} \tag{4.2.6}$$

For a measurement system that resolves each element of the retrieved state vector with perfect sensitivity, $\mathbf{A}$ equals the identity matrix. The 'n' row of $\mathbf{A}$ then corresponds to a delta function response to the n element of the retrieved state vector. The 'n' column of $\mathbf{A}$ is the impulse response to a perturbation in the element of the true state

vector. In ground-based FTIR measurements the diagonal elements of $\mathbf{A}$ are not unity (representing imperfect sensitivity to the true state at all heights) and off-diagonal elements are present (representing the inability to independently resolve all element of the retrieved state vector). The above results are strictly valid where the measurement and state vectors are linearly related and where the measurement and a priori error covariance statistics are Gaussian '$P(y) = \frac{1}{\sqrt{(2\pi)^n S_y}} \exp\left(\frac{-1}{2}(y-\bar{y})S_y^{-1}(y-\bar{y})\right)$'. More commonly the forward model $\mathbf{K}$ is only a linearization about a reference state, here taken to be the a priori state ($\mathbf{K} = \frac{\partial \mathbf{F}}{\partial \mathbf{x}}$ is a matrix of derivatives evaluated at the reference state) [18]. In this case the optimal solution is obtained using Newtonian iteration and is given by

$$\mathbf{x_{i+1}} = \mathbf{x_a} + (\mathbf{K_i^T S_\epsilon^{-1} K_i} + \mathbf{S_a^{-1}})^{-1} \mathbf{K_i^T S_\epsilon^{-1}} [(\mathbf{y} - \mathbf{y_i}) - \mathbf{K_i}(\mathbf{x_a} - \mathbf{x_i})] \tag{4.2.7}$$

where $\mathbf{K_i}$ is taken to mean '$\mathbf{K}$ evaluated at $\mathbf{x_i}$' and $\mathbf{y_i} = \mathbf{F}(\mathbf{x_i})$.

The number of state vector elements that are independently resolved is calculated by taking the trace of $\mathbf{A}$ and is referred to as the degrees of freedom for signal in the measurement

$$\mathbf{d_s} = \mathbf{tr}(\mathbf{A}) \tag{4.2.8}$$

By taking the trace of $\mathbf{A}$ over a certain vertical range of the atmosphere, we determine the number of independently resolved pieces of information present in the partial column derived from this region. The information content may be defined in terms of the degrees of freedom for signal which is the trace of the averaging kernel. Mathematically this is the sum of the diagonal elements of the averaging kernel matrix [19]. The characterization of vertical information contained in high-resolution FTIR spectra is of ongoing interest to the IDACC; the more sophisticated vertical profile and partial column data products clearly have more uses in basic research and satellite validation applications than the more limited vertical columns.

The retrieval code we used for Optimal Estimation Method (OEM) retrieval algorithm

is PROFFIT developed by F.Hase [22]. The first step in our retrieval is to calculate a model atmosphere forward calculation (PROFFWD) which provides synthetic and measured spectrum and derivatives for error estimation. This software performs a radiative transfer calculation for a given set of relevant atmosphere (T, p, VMRs). Pressure and temperature dependent absorption line parameters are obtained from the high-resolution transmission molecular absorption (HITRAN) and auxiliary (SZA, ILS) input quantities for the spectral microwindows are selected for analysis. The derivative of the spectrum with respect to the target and auxiliary quantities are allowed to vary in the process of searching the best estimate of the atmospheric state. The second step, the inversion model (PROFFIT), which processes the PROFFWD model output and suggests improved solution, restarts forward model with updated variables, cycles until convergence is reached. In short, PROFFIT determines a best estimate of the observed atmospheric state by improving fit quality to recorded spectrum iteratively.

Chapter 5

FTIR Spectrometer in AAU

Introduction

Spectroscopic measurement techniques are well suited for remote sensing of the atmosphere. As solar radiation passes through the atmosphere, trace gases selectively absorb at specific wavelengths of the light. The measurement of the sun's spectrum at the Earths surface thus provides a wealth of information about atmospheric composition (see Fig.5.1). Such experiments make use of the Sun as a light source to quantify molecular absorptions in the atmosphere and then retrieve trace gases abundance [23]. Stratospheric ozone, other trace and greenhouse gases are routinely measured with this technique from ground-based FTIR spectrometers. The high-resolution FTIR Spectrometer, Bruker IFS120M, from Bruker Optics Company in Germany is installed in May, 2009 at Addis Ababa, in the Science Faculty Campus of AAU with collaboration of the Karlsruhe Institute of Meteorology and Climate Research, currently called KIT found in Germany. This instrument is the first of its kind in Africa. For optimum spectrometer performance and long-term reliability, the instruments operates at stable temperature of 20^0C, which is maintained by air conditioner. As the instrument is the first in our country, it is important to report the set up of the instrument and measurement performance of the instrument. Next we introduce some of the main parts of the instrument briefly but we begin by solar tracker.

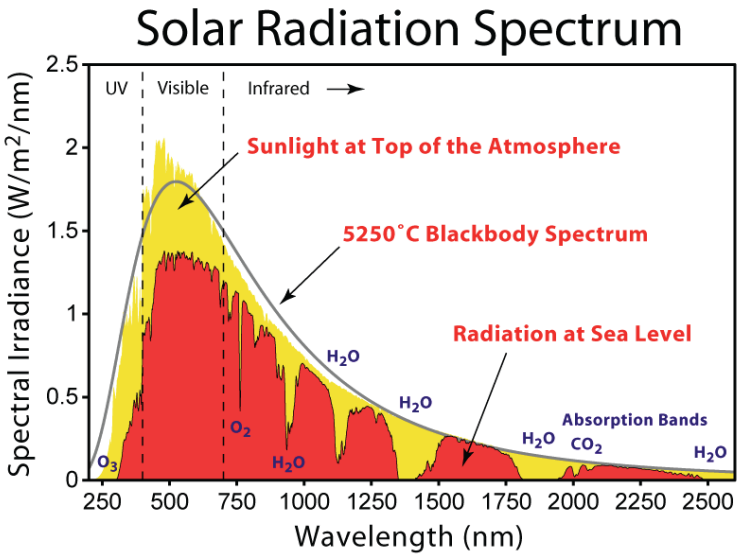

Figure 5.1: Solar spectrum at the top of the atmosphere, at sea leval, and the Planck curve of a black body at T=5250^{0}C (temperature of the sun).

5.1 FTIR Components

5.1.1 The solar tracker

The solar tracker is need to follow the sun and directed beam into the spectrometer. It is a tripod that has a reflecting mirror at head facing to the sun and moving with the 'speed of the sun'. It has a motor to provide a constant power so that the incoming solar radiation is reflected from the plane mirror of this to another plane mirror inside the container through the infront window which in turn reflects the beam to interferometer passing through aperture of size of interest. The tracker in our site of Addis Ababa is not interfaced with the instrument and computer. First of all we align the tripod elevation and azimuth to the north star(polaris) direction at night during clear sky time to assure stabilization of the tracker. After this the incoming solar radiation simply reaches to the aperture so we measure the radiation of the filters for ten scan times for each measurment.

Filter	*Wavenumber* (cm^{-1})	*Wavelength* (μm)
1	$4000 - 4300$	$2.3 - 2.5$
2	$2900 - 3500$	$2.6 - 3.3$
3	$2400 - 3100$	$3.3 - 4.1$
4	$2000 - 2700$	$3.9 - 5.0$
5	$1500 - 2200$	$4.7 - 6.3$
6	$750 - 1350$	$7.4 - 14$

Table 5.1: Spectral Coverage of the IFS120M instrument at Addis Ababa site.

5.1.2 The Optical Devices

The optical components of the FTIR are the most sensitive parts of the instrument. It consists of parabolic mirrors (parabolloids) that uses to focus the beam of sunlight on to aperture and to transform the beam into parallel rays; **aperture** is used to limit the field of view and also the intensity of incoming radiation as per choice of the operator. Note that the self apodization (interference of light emerging from the aperture due to finite aperture size) depend on its size when the smaller the aperture size, the lesser self apodization; **filters** serves as to limit the wavenumber range of as per our interst. It is responsible for channeling and any leakage of the filter that can be seen on baseline of the measured spectrum. Our IFS120M instrument has two sets of filter wheels that has six separate filters. The spectral coverage of these filters have overlaps in order to guarantee the possibility of retrieval using lines in one extreme of the filter coverage; and the band coverage for each filter is given in **Table** 5.1. These filter ranges are also used by IDACC. The **beamsplitter** must preserve in good enviromental condition because of highly sensitivity to expire and also expensive cost. It is a heart of the interferometer that used for splitting the incident light beam into two parts, one by reflecting to a fixed mirror other by transmitting to movable mirror (retro- reflector). Both split beams are reflected by the mirrors (fixed and moveable) and travel back to the beamsplitter after moving different path length then recombine they are recorded by the detector. We have two beamsplitter in the FTIR room one **KBr** the other is

CaF_2 that shown in Fig. 5.2. KBr is highly hygroscopic and it's recommended not to use during rainy season and put it in a dry, warm places. It is kept in a beamsplitter storage glass jar to protect it from exposure to humidity.

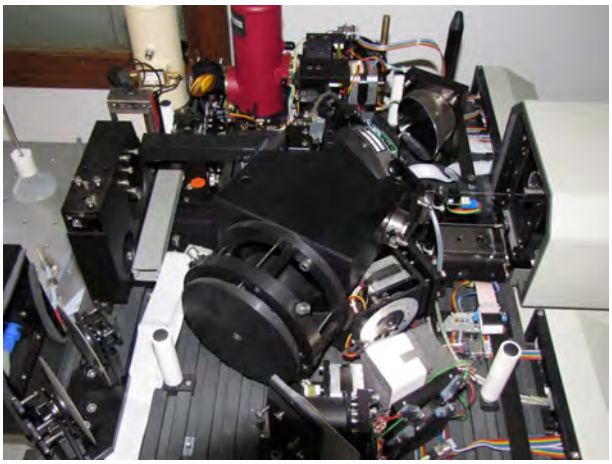

Figure 5.2: The IFS120M instrument optical set up and beamsplitters in Addis Ababa.

5.1.3 The Detectors

The infrared detector is a device which measures the infrared energy of the source which has passed through the spectrometer. Detectors change radiation energy into electrical energy which can be processed to generate a spectrum. There are two basic types, thermal detectors or photon detectors according to their working principles. Thermal detectors exhibit a change in some measurable electrical property that accompanies a change in temperature of the sensitive element, caused by absorption of radiation by the sensitive element. For example, the Silicon bolometer detector-depends on a change of resistance with temperature, and the pyroelectric detector consists of a thin pyroelectric crystal such as DTGS operates at room temperature. Being a thermal device, it possesses essentially flat wavelength response ranging from the near-IR through the far-IR. It can handle signal frequencies of upto several thousand Hertz and hence is well suited for Fourier transform infrared spectrometers. Photon detectors are also called

quantum detectors. This category of detectors is based on the creation of charge carriers (electron-hole pairs) in a semiconductor material due to absorbed electromagnetic radiation, followed by subsequent collection and amplification of the charges created. Photon detectors are more sensitive, and have fast response times. They usually operate below or at liquid nitrogen temperatures. Photon detectors include **MCT**, **InAs** and others. These detectors utilize photon energy to promote bound electrons in the detector material to free states, which results in increased electrical conduction [20].
It is one of the central part of IFS120M Bruker spectrometer, in our FTIR room there are two detectors that made up of **(MCT)** and **(InAs)** alloys. The InAs detector covers a spectral range of (1,850-9,600) cm^{-1} and the MCT covers (750-5,000) cm^{-1} while both effectively operate at a temperature $\leqslant 70K$ attained by filling the detector dewar by liquid nitrogen(N_2). In our instrument, we usually use InAs detector to cover spectral range from $1800-4200\ cm^{-1}$ using five filters, and MCT for $780-2000\ cm^{-1}$. Both types of detectors operated in Photo-voltaic principle while the InAs is a linear detector. That is, both the MCT and InAs elements absorb IR photons, and as a result electrons are promoted from the valence band to conduction band, and give rise to an electrical current. The current is then a direct measure of infrared(IR) intensity which increases with the number of IR photons. The disadvantage of MCT over InAs is its easy saturation, which results in non-linearity of detector response for incoming radiation. A perfectly linear detector should produce a spectrum with all saturated absorption features at zero, because there is no radiation of these wavelengths reaching the detector.

$Filter$	$Resolution\ (cm^{-1})$	$No.of Scans$	$Detector$
$1-5$	0.009	10	$InAs$
6	0.009	10	MCT

Table 5.2: Measurement parameters used in the IFS120M instrument at AAU.

5.1.4 The Scanner

It is the only moving part of FTIR spectrometer that holds a movable mirror and moves back and forth. The mirror, driving cables and two driving units constitute the main part of FTIR scanner. The two driving units of the scanner are 1 DC motor and 1 linear drive unit. The two driving units are also called the outer and inner scanners [16]. The outer scanner ensures the gliding movement of scanner, and the main function of the inner scanner is to compensate the fluctuations of the outer scanner, same purpose as fine tuning in radio. The position of the moving mirror is precisely controlled by stabilized He-Ne laser signal (631.8 nm), so that the optical path difference can be measured accurately. The laser signal is also used to determine the data sampling positions. In our IFS120M we get more than 2100000 data points from $0-4000$ wavenumber intervals. If the scanner moves with uniform speed, the sinusoidal signal is generated as a result of modulation of He-Ne laser, and this generated signal reaches the detector (either InAs or MCT). The intensity of the interfering beams (after reflection from the fixed and moving retroreflector and recombined at the beamsplitter) is measured as a function of OPD, and the result is an interference pattern, called interferogram. Note that, the beam splitter, retro-reflectors, and detector constitute the main components of interferometer. The angle of incidence of the beam to the interferometer is 30^0 [17]. This narrow angle of incidence reduces polarization effects and uses the beam splitter more efficiently [16].

5.1.5 The IR sources

The InfraRed source in FTIR is used to provide IR radiation to the spectrometer. In our FTIR, we use glow bar (globar), it is a piece of ceramic usually rod of silcon carbide. When electric current passes through it, the resistance of the device makes it heat up and give off IR radiation. The globar may heat above 1400 K, so that we can get more

IR radiation, which in turn results in higher throughput and lower noise in our FTIR spectra. The globar compartment is supplied with a closed-loop cooling system, where the cooling unit accommodate about half-a-litter of water for this purpose. The cooling unit must be filled with distilled or deionized water only; and it is recommended to change the water at least once every three months. The globar is mainly used for the calibration of the FTIR by means of a black body, and also to align optical device to get maximum radiation at the detector. In order to determine the ILS, which tells us the status of the instrument, we take black body radiation with globar source and the radiation passes through a low-pressure gas cell filled with HBr, which has sharp absorption lines.

5.1.6 The Electronics Unit

The electronics unit of an FTIR is used to convert optical signals into electrical signals. The intensity of IR photons reaching the detector is converted into electrical current by the electronics unit and send to monitor (PC). The electronics unit is also used to calibrate the IR wavenumber with respect to the laser wavenumber Some of the jobs carried out by electronics units is the ADC, phase correction, pre-amplification of the raw data (Interferogram) and ACR. The IFS120M instrument is controlled by a PC data system, provided the $Microsoft\ windows^{TM}$ operating system and the $OPUS^{TM}$, which is a spectrometer software, installed on PC to take measurement, and for analysis of the spectra. The ethernet connection allows to control status of the spectrometer components via internet. The interference between the two secondary beams (Interferogram) is digitized and sent to PC where the FT takes place using OPUS software to get the final infrared spectrum for analysis.

Chapter 6

Principle of FTIR Spectrometry

6.1 Ideal Fourier Transform Spectrometer

The heart of the optical hardware in a FT spectrometer is the interferometer. Nowadays, the most common set-up used is the classic two-beam Michelson interferometer shown schematically in Fig. 6.1. A beam emitted by a source **S** is split in two by the beam splitter. The reflected part of the beam travels to the fixed mirror $\mathbf{M}_1$ through the distance **L**, is reflected there and hits the beam splitter again after the total path length of 2L. The same happens to the transmitted radiation. However, as the mirror $\mathbf{M}_2$ is not fixed at the same position L but can be moved very precisely back and forth around L by a distance **x**, the total path length of the transmitted part is accordingly $2(L + x)$. Thus, when the two parts of the beam recombine at the beamsplitter they possess an optical path length difference of $\delta = \mathbf{2x}$ Since the two split beams are spatially coherent, they interfere on recombination. Naturally, only half of the radiation entering the interferometer can get out in the out direction; half is reflected back towards the input. Because of the effect of interference, the intensity of each beam passing the detector and returning to the source depends on the difference in path of the beams. The spectrum sent to the detector is the product of the two interfering beams, depending on the path difference M_1 and M_2 [21].

In the case of a monochromatic ray, the two bundles of radiation interfere constructively if their optical retardation is a multiple of the wavelength λ, i.e.

$$if \quad \delta = 2x = n\lambda \quad with \quad n = 0, 1, 2, 3, ... \tag{6.1.1}$$

and destructively if λ is an odd multiple of $\lambda/2$, i.e.

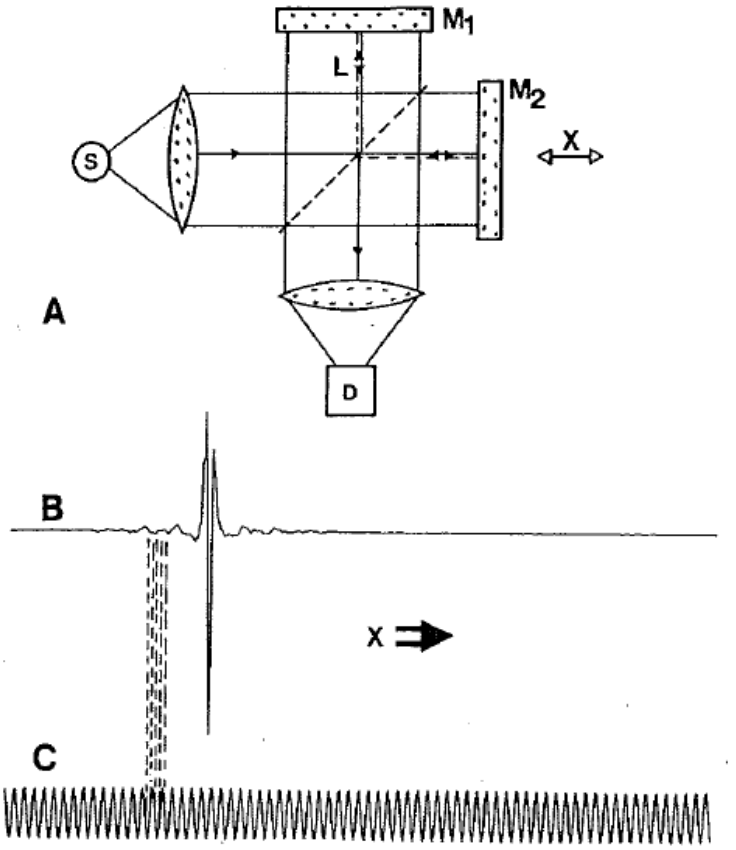

Figure 6.1: A)The schematic of a Michelson interferometer, B)Interferogram and C)Interferance pattern of a laser source.

$$if \quad \delta = 2x = (2n + 1)\frac{\lambda}{2} \tag{6.1.2}$$

The beam, modulated by the movement of the mirror M_2, leaves the interferometer and is finally focussed on the detector. The signal actually registered by the detector is thus the radiation intensity of the combined beams as a function of the retardation δ. For a source of monochromatic radiation with frequency ν (or wavenumber, $\tilde{\nu} = \frac{1}{\lambda} = \frac{\nu}{c}$),

the intensity at the detector **(D)** measured with an ideal interferometer is given by the equation

$$I_D(\delta) = 0.5S(\tilde{\nu})[1 + \cos(2\pi\tilde{\nu}\delta)] \tag{6.1.3}$$

where $S(\tilde{\nu})$ is the intensity of the monochromatic beam. It can be seen that $I_D(\delta)$ is composed of a constant (DC) component and a modulated (AC) component. Only the AC component is important in spectroscopic measurements, and it is this modulated component that is generally referred to as the interferogram:

$$I_D(\delta) = S(\tilde{\nu})\cos(2\pi\tilde{\nu}\delta) \tag{6.1.4}$$

Eq. (6.1.4) is extremely useful for practical measurments, because it allows very precise tracking of the movable mirror. In fact, all modern FT-IR spectrometers use the interference pattern of the monochromatic light of a He-Ne laser to control the change in optical path difference. This demonstrates how the IR interferogram is digitized precisely at the zero crossings of the laser interferogram. As the retardation is a function of time, the interferogram is a function defined in the time domain. If the movable mirror is scanned at a constant velocity v, the retardation is simply

$$\delta = 2vt \tag{6.1.5}$$

and the interferogram $I(t)$ is given by

$$I(t) = S(\tilde{\nu})\cos(2\pi\tilde{\nu}2vt) \tag{6.1.6}$$

Therefore, the signal at the detector varies sinusoidally with the frequency

$$f_{\tilde{\nu}} = 2v\tilde{\nu} \tag{6.1.7}$$

For a source of polychromatic radiation the interference pattern is given by, a superposition of such cosines

$$I(\delta) = I_D(\delta) - \bar{I}(\delta) = \int_0^\infty S(\tilde{\nu})cos(2\pi\tilde{\nu}\delta)d\tilde{\nu} \tag{6.1.8}$$

where $\bar{I}(\delta)$ is the constant part, the mean value can be substracted to form an expression for the intensity as a function of δ and $S(\tilde{\nu})$ is now the spectral power density of the source. An interferogram is characterised by a "centre burst" at zero path difference and a very complex pattern of waves symmetrically dispersed about it. The optical retardation that corresponds to the maximum displacement, δ_{max}, determines the theoretical limiting resolution of the interferometer. In practice the resolution is never attained because of truncation or apodization.

Data acquisition yields the digitized interferogram which must be converted into a spectrum by means of mathematical operation called Fourier transformation (FT). Accordingly, the spectrum is given by

$$S_L(\tilde{\nu}) = \int_{-\infty}^{\infty} I(\delta) cos(2\pi\tilde{\nu}\delta) d\delta \tag{6.1.9}$$

Mathematecilly, the Fourier transform of Eqn (6.1.8) produce not only the spectrum $S(\tilde{\nu})$ but also its mirror image, $S(-\tilde{\nu})$, at negative frequencies. Since $cos(2\pi\tilde{\nu}\delta) = cos(-2\pi\tilde{\nu}\delta)$, $S(\tilde{\nu})$ and $S(-\tilde{\nu})$ produce identical interferograms. The negative frequencies are physically unreal. For complete symmetry in transforming back and forth from the interferogram domain to the spectral domain, the integral has to extend over all frequencies from minus to plus infinity. It is possible to construct a spectral function $S_L(\tilde{\nu})$ from $S(\tilde{\nu})$ and change the definition to include all frequencies:

$$S_L(\tilde{\nu}) = \frac{1}{2}[S(\tilde{\nu}) + S(-\tilde{\nu})]$$

$$I(\delta) = \int_{-\infty}^{\infty} S_L(\tilde{\nu}) cos(2\pi\tilde{\nu}\delta) d\tilde{\nu}$$

In practice, the interferogram measured is not mirror symmetrical about the point $\delta = 0$. This asymmetry originates from experimental errors, e.g., wavenumber dependent phase delays of the optics, the detector /amplifier unit, or the electronic filters. The Fourier transformation of such an asymmetrical interferogram generally yields a

complex spectrum $C(\tilde{\nu})$ rather than a real spectrum $S(\tilde{\nu})$, A complex spectrum $C(\tilde{\nu})$ can be represented by the sum [21]

$$C(\tilde{\nu}) = S(\tilde{\nu}) \exp\left(i\Phi(\tilde{\nu})\right) \tag{6.1.10}$$

of the 'amplitude' spectrum $S(\tilde{\nu})$ and the complex exponential function $\exp\left(i\Phi(\tilde{\nu})\right)$ containing the wavenumber-dependent 'phase' $\Phi(\tilde{\nu})$:

$$C(\tilde{\nu}) = S(\tilde{\nu})cos(\Phi(\tilde{\nu})) + iS(\tilde{\nu})sin(\Phi(\tilde{\nu}))$$

$$C(\tilde{\nu}) = \Re_{Real}(\tilde{\nu}) + iI_{Imaginary}(\tilde{\nu})$$

The purpose of the phase correction procedure is to determine the amplitude spectrum $S(\tilde{\nu})$ from the complex output $C(\tilde{\nu})$of the FT of the interferogram. This can be performed either by calculating the square root of the 'power' spectrum

$$S(\tilde{\nu}) = \sqrt{R^2(\tilde{\nu}) + I^2(\tilde{\nu})}$$

or by multiplication of $C(\tilde{\nu})$ by the inverse of the phase exponential and taking the real part of the results:

$$S(\tilde{\nu}) = C(\tilde{\nu}) \exp\left(-i\Phi(\tilde{\nu})\right)$$

In general, in IR spectroscopy, the interferogram and spectrum are related by a general Fourier transformation.

6.1.1 Discrete Fourier Transform

A laser-controlled FT spectrometer, the interferogram is digitised and consists of **N** discrete, equidistant points. That means that instead of Eqn(6.1.9) we have to use the discrete Fourier transformation [21]:

$$S(k.\Delta\tilde{\nu}) = \sum_{n=0}^{N-1} I(n\Delta x)\exp(2\pi ikn/N) \tag{6.1.11}$$

where the continuous variables δ and $\tilde{\nu}$ have been replaced by $n.\Delta x$ and $k.\Delta\tilde{\nu}$, respectively. The spacing $\Delta\tilde{\nu}$ in the spectrum is related to Δx by

$$\Delta\tilde{\nu} = \frac{1}{N.\Delta x} \tag{6.1.12}$$

Alternatively, if the set $S(k\delta\tilde{\nu})$ of Fourier coefficients is known, one can easily reconstruct the interferogram $I(n.\Delta x)$ with the computer by the inverse discrete Fourier transformation:

$$I(n\Delta x) = (1/N)\sum_{k=0}^{N-1} S(k\Delta\tilde{\nu})\exp(-2\pi ink/N) \tag{6.1.13}$$

In practice, Eqn(6.1.10) is seldom used directly because it is highly redundant. Instead most manufacturers apply the so-called FFT algorithm, preferably according to Cooley and Tukey algorithm. The aim of this FFT is to reduce the number of complex multiplications and sine and cosine calculations appreciable, leading to a substantial saving of computer time. The price (small) paid for the speed is that the number of interferogram points N cannot be chosen at will, namely N must be a power of two. For this reason and from the relation of Eqn(6.1.11), it follows that the spectra recorded with laser-controlled FT spectrometers exhibit a sampling spacing of $\Delta\tilde{\nu} = \frac{m}{2^N}\tilde{\nu}_{laser}$.

6.2 Real FT Spectrometer

The real spectrometer is the one with finite Optical Path Difference 'δ' and the interferogram is sampled only with finite step size Δx. It is not possible to calculate $S(\tilde{\nu})$ from Eqn(6.1.9) because the integration limits require infinite mirror displacement. The performance of the FT spectrometer is measured in terms of ILS, modulation efficiency and phase error as a function of optical path difference [18].

6.2.1 ILS and Apodization function

Eqn(6.1.9) shows that in order to measure the complete spectrum, we would have to scan the moving mirror of the interferometer an infinitely long distance, with δ varying between $-\infty$ and ∞ centimeters. It must be finite mirror movement $\delta = \pm L\ cm$, the resulting IR spectrum will have a finite resolution of $\frac{1}{2L}\ cm^{-1}$ so that the equation is rewritten as

$$S_L(\tilde{\nu}) = \int_{-\infty}^{\infty} I(\delta)D(\delta)\cos(2\pi\tilde{\nu}\delta)d\delta \tag{6.2.1}$$

where $D(\delta)$ is denoted as an apodization function.

Therefore apodization function is a function (also called a tapering function) used to bring an interferogram smoothly down to zero at the edges of the sampled region. This suppresses sidelobes which would otherwise be produced, but at the expense of widening the lines and therefore decreasing the resolution.

There are different types of apodization functions that differ significantly regarding with side-lobe intensity: boxcar, Triangular, Welch, etc. However the results reported here were obtained using the boxcar truncation function. The boxcar function is the most simple function, and preserves the maximum of information from the interferogram, but introduces side lobes. The boxcar truncation function

$$D(\delta) = \begin{cases} 1 & \text{if } : -L \leq \delta \leq L, \\ 0 & \text{if } : \delta > |L|. \end{cases} \tag{6.2.2}$$

According to the convolution theorem of Fourier analysis, the Fourier transform of a product of two functions is given by the convolution of their individual Fourier transforms [21]. The Fourier transform of $I(\delta)$ is the true spectrum $S(\tilde{\nu})$, while the Fourier transform of $D(\delta)$, $f(\tilde{\nu})$, is given by

$$f(\tilde{\nu}) = \frac{2l\sin(2\pi\tilde{\nu}l)}{2\pi\tilde{\nu}l} \tag{6.2.3}$$

This Fourier transform of a monochromatic source is not an infinitely narrow line, but has the shape of the sinc function, as shown in Fig. 6.2. Therefore, the spectrum $S_l(\tilde{\nu})$

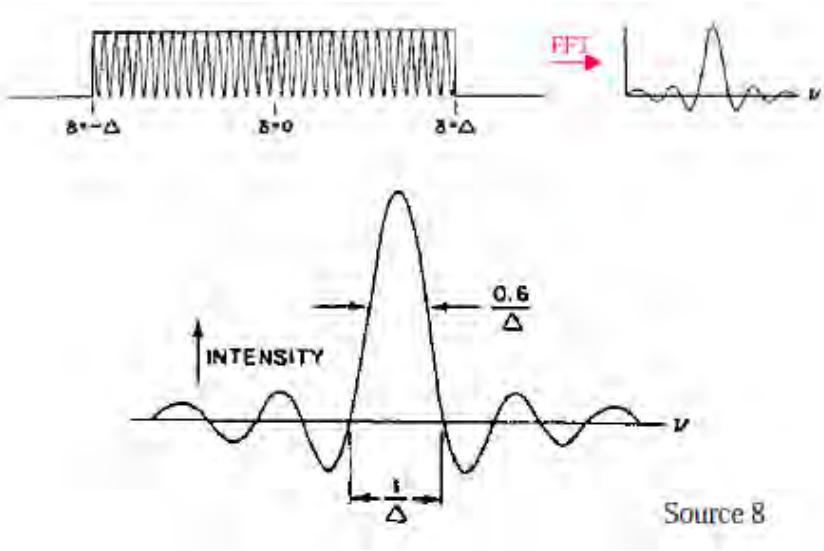

Figure 6.2: Upper: Boxcar truncation multiplying the interferogram by rectangular function. lower: ILS of boxcar truncation after Fourier transformation is applied showing FWHM.

measured with a finite length retardation is described by

$$S_L(\tilde{\nu}) = S(\tilde{\nu}) \otimes f(\tilde{\nu}) \tag{6.2.4}$$

where, $f(\tilde{\nu})$ is the Fourier transform of boxcar function, also known as the ILS. The ILS is very important because it guides for right and correct conclusions from the measurements characterizing the instrument performance. ILS gives an accurate knowledge about the spectral resolution over the measurements. So it enables a clear description of a measured lineshape in terms of a natural lineshape due to physical line broading, the ILS representing solely the contribution of finite resolution.

The limited optical path difference leads to sinc function with Full Width at Half Maximum, yields a resolution of

$$\triangle_{FWHM} = \frac{0.605}{L} \tag{6.2.5}$$

We use this criterion conventionally, however the resolution is expected to be higher

for usage of boxcar apodization. The other thing which affects ILS is the so called self apodization. Self-apodization is due to finite field of view of the spectrometer, i.e., finite aperture. Comparing the true resolution of two spectra calculated from the same interferogram by using either boxcar or triangular apodization, the loss in resolution for triangular apodization is 47% to real ILS. The real ILS of our IFS120M instrument is determined nearly regularly from low pressure gas cell measurement which is filled with HBr. We usually use the wavenumber range of IDACC filter 3 range which covers from 2400 to 2700 cm^{-1}. Our radiation source is a globar of about 1273 K and we used the latest version of LINEFIT (Version12) software to retrieve ILS.

In our case, the maximum OPD is 250cm, but due to some reasons we limited the maximum OPD to 100cm only and it can attain a resolution of $0.009cm^{-1}$ using boxcar apodization. The spectral half width of an ideal monochromatic line after triangular apodization is used to specify spectral resolution which is a common practice by commercial FTS manufacturers like BRUKER Optics, which is given by

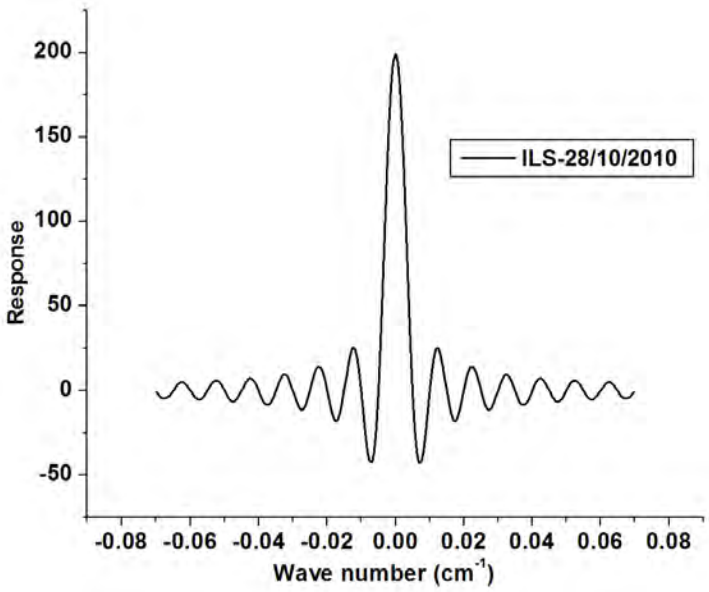

Figure 6.3: Retrieved ILS of the IFS120M in Addis Ababa, for 28/10/2010/

$$\triangle \nu = \frac{0.9}{OPD_{max}} \tag{6.2.6}$$

Fig. 6.3 shows the retrieved ILS of IFS120M for the HBr cell measurement taken on October 28, 2010. As it is seen from Fig. 6.3 the true ILS resembles the ideal ILS shown in Fig. 6.2. The comparison of the true and ideal ILS's will be done using the modulation effciency loss and phase error evolution. The real ILS differs from the ideal ILS which is determined by the applied apodization function and the self-apodization due to the non perfect alignment.

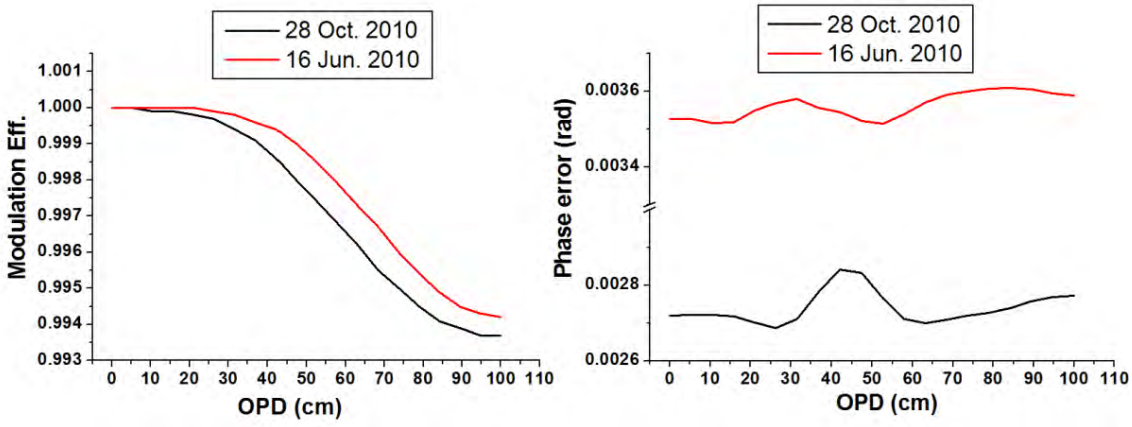

Figure 6.4: ILS parameters: (Left panel) Modulation Efficiency and (Right Panel) Phase Error for 16/06/2010 and 28/10/2010.

Next we show the evolution of ILS since the first measurement date of our IFS 120M instrument. As we mentioned before the performance of the instrument is measured in terms of the modulation efficiency and phase error. The sample (cell) and background spectra were measured, and then the ratio of spectrum with sample over the background spectrum was in order to obtain the real transmittance spectrum.

The resulting maximum phase error on 16/06/2010 was in the order of 3.61×10^{-3} rad and on 28/10/2010 in the order of 2.85×10^{-3} rad for maximum path difference. There was linear modulation efficiency losses of 0.006 for the two days around (see Fig. 6.4). This shows that the instrument's alignment has been improved since the beginning of the measurement time [17].

Finally, we would like to discuss the spectral fits of the measurement on 28 october,

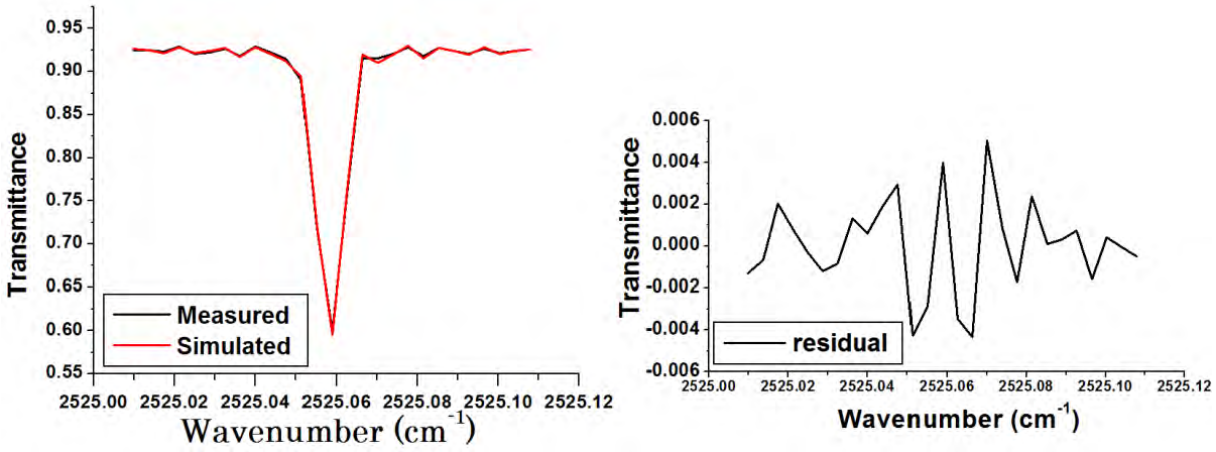

Figure 6.5: The measured and simulated transmittance spectral fit from HBr cell measurement (Left panel) and the corresponding residual spectra between the measured and calculated spectra (Right panel) on 28/10/2010.

2010. Fig. 6.5. shows the HBr spectral fit for the indicated wavenumber region. The left panel is a plot of the measured and calculated transmission spectra and the right panel is the residual between the two spectra with a resolution of $0.008cm^{-1}$. For this the ILS, modulation efficiency and phase error corresponding to this spectral fit has been shown in Figs. 6.4. The root-mean-squared value of the noise is below 1%. We can judge from the figure that the residual is a random noise.

Chapter 7

Results and Discussion

The Addis Abeba FTS Observatory is located at 9.01^0N, 38.76^0S and $2450m$ above sea level. FTIR solar absorption spectra are recorded under clear-sky conditions, 8 to 10 minute constructed by co-adding up to 10 scans. The number of observation days for NO is 76 and 113 for NO_2. FTIR data set used for this study covers days from 14 May, 2009 to 05 February, 2011. The temporal coverage of the dataset is more sparse in the winter months. Towards the end of this chapter we show that the validation of NO_2 total column amount with OMI level3 NO_2.

7.1 Retrieval strategy and spectral fits

In this section, we give an overview of our retrieval approach for NO and NO_2 retrieved on 41 layer atmosphere, from 2.45 km up to 85 km altitude. The measured spectra are analyzed with the inversion code PROFFIT [22].

Table 7.1 gives a summary of the selected retrieval microwindows, the mean effective SNR, interfering molecules, and the achieved average DOFs for the two target species, at Addis Ababa from May, 2009 upto February, 2011.

7.1.1 Spectral micro-window selections

The micro-windows in which NO and NO_2 are retrieved, as well as the interfering absorbers whose total columns are fitted simultaneously with the target species, have been adopted from spectral microwindows used by Izana FTIR research groups and modified slight in order to improve our retrievals [24]. Modifications were carried out using softwares called ALFIP and INTDIF. ALFIP calculates the spectra and finds the most suitable lines and optimized microwindow size.

Table 7.1: Microwindows and interfering species used in operational AAU retrievals with average SNR and degrees of freedom for signal.

Target gas	Micro-window(s) cm^{-1}	SNR	Interfering species	DOFs
NO	1899.880 -1900.200 1903.100 -1903.160 1928.980 -1929.044	352.62	H_2O, CO_2	1.18
NO_2	2888.250 -2888.311 2893.290 -2893.360 2914.536 -2914.755	2863.92	H_2O, CH_4	1.05

7.1.2 Construction of a priori information and retrieval results

Generally, a priori profiles of the interfering species are taken from climatology. In the retrieval procedure, these profiles are scaled together with the inversion of the target gas profile. The apriori profiles for both target gases (NO and NO_2) and interfering trace species were taken from tropical climatological apriori profiles of Remedious. A priori profiles of pressure and temperature taken from the NCEP reanalyses available through the NASA Goddard Space Flight Center automailer ($http$: $//hyperion.gsfc.nasa.gov/Dataservices/automailer/index.html$) and spectral parameters taken from the HITRAN database. The left bottom panel in Fig. 7.1 shows 1^{st} micro-window fit of NO from a single spectrum on 26 November 2009, with the residuals error (left upper panel), and the right panel in Fig. 7.1 shows 3^{rd} micro-window

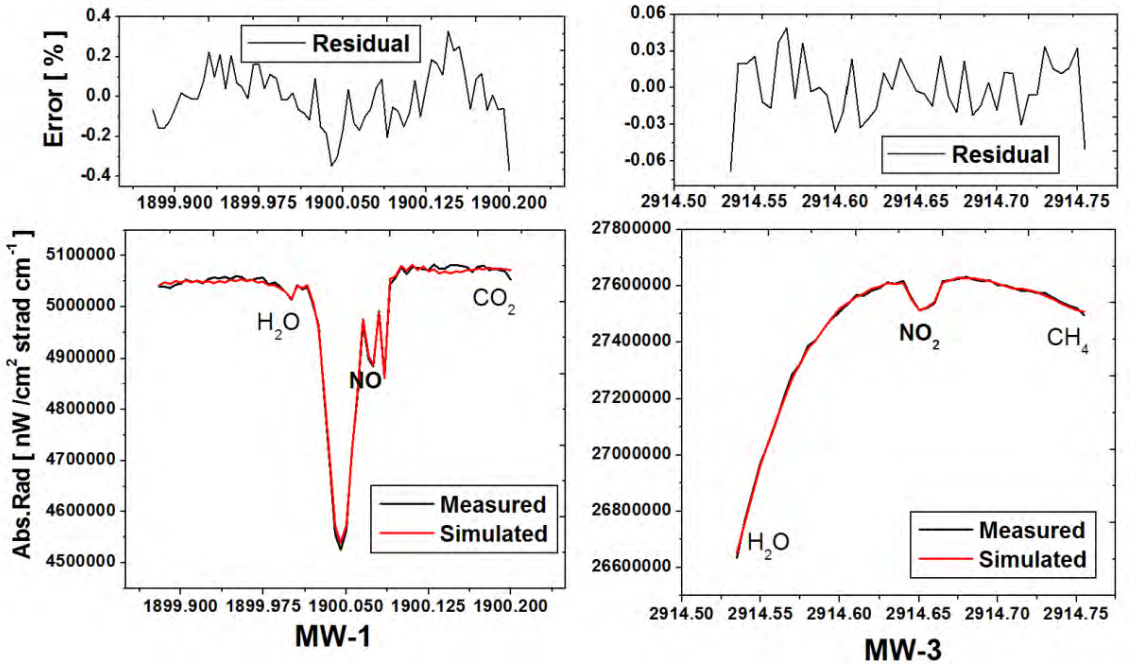

Figure 7.1: Measured and simulated spectra for both gases:[left panel] MW-1(1899.000-1900.200) fit of NO plus interfering species from a single spectrum on 26 November 2009 and [right panel] MW-3(2914.536-2914.755) fit of NO_2 plus interfering species from a single spectrum on 30 May 2009.

fit of NO_2 from a single spectrum on 30 May 2009, with the residuals (right upper panel). The maximum residual for all microwindows spectral fit is less than 4×10^{-3} (or 0.4%), for NO and 8×10^{-4} (or 0.08%) for NO_2. The noise in the residuals is primarily random with small systematic features near the peak absorption of the both target gases and interfering gases. The residual error of NO comes mostly from the interfering gases, H_2O and CO_2 and for NO_2 from H_2O and CH_4. This noise has an important impact on the quality of the measurement. NO and NO_2 average SNR is 352.62 and 2863.92 respectively (see Table 7.1). It indicates good fit quality.

Vertical information in retrievals from FTIR spectra

The vertical information contained in the retrievals can be characterized by the averaging kernel matrix in Eqn(4.2.6). This matrix depends on measurement and retrieval parameters including the SZA, the spectral resolution and signal to noise ratio, the

choice of spectral microwindows, and the a priori covariance matrix. Figs. 7.2 and 7.3 show the rows of the averaging kernels matrix for a typical profile retrieval of NO_2 and NO on the 41-layer height grid respectively. They indicate, at each altitude, the fraction of the retrieval that comes from the measurement rather than from the a priori information. A value close to zero at a certain altitude indicates that the retrieved profile at that altitude is nearly independent of the real profile and is therefore approaching the a priori profile. So the integrated area under each averaging kernel is a simple measure of the amount of non-a priori information that appears in the retrieval at the corresponding height. It is clear that the retrieval is most sensitive in stratosphere and upper troposphere for NO_2 between 15 and 38 km. Also the retrieval is most sensitive in stratosphere and upper troposphere for NO between 11 and 44 km. From daily NASA(Goddard) meteorological data tropopause hight over Ethiopia is around 17 km.

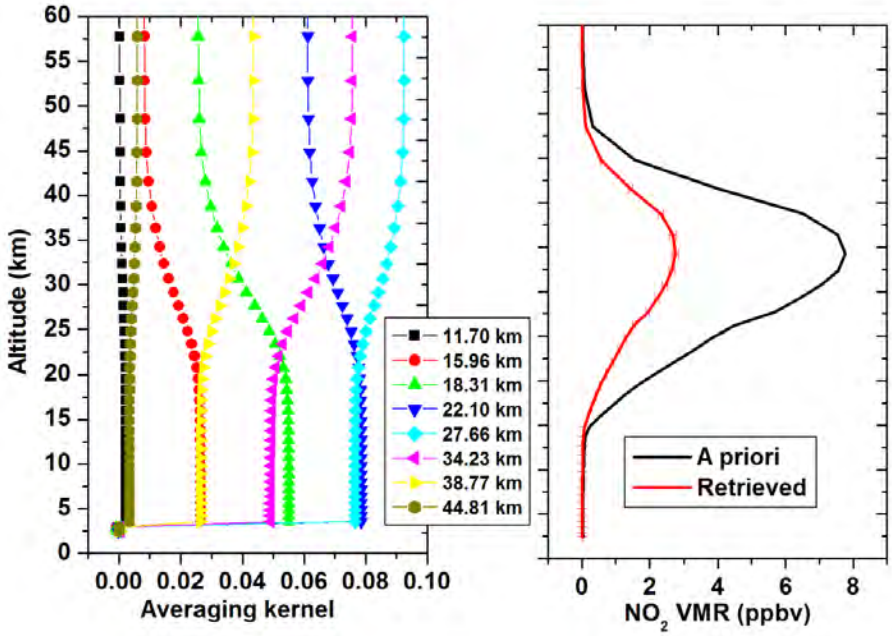

Figure 7.2: [Left panel] Averaging kernel of NO_2 for selected heights and [Right panel] retrieved profile on 30 May 2009 at a SZA of 49.07^0.

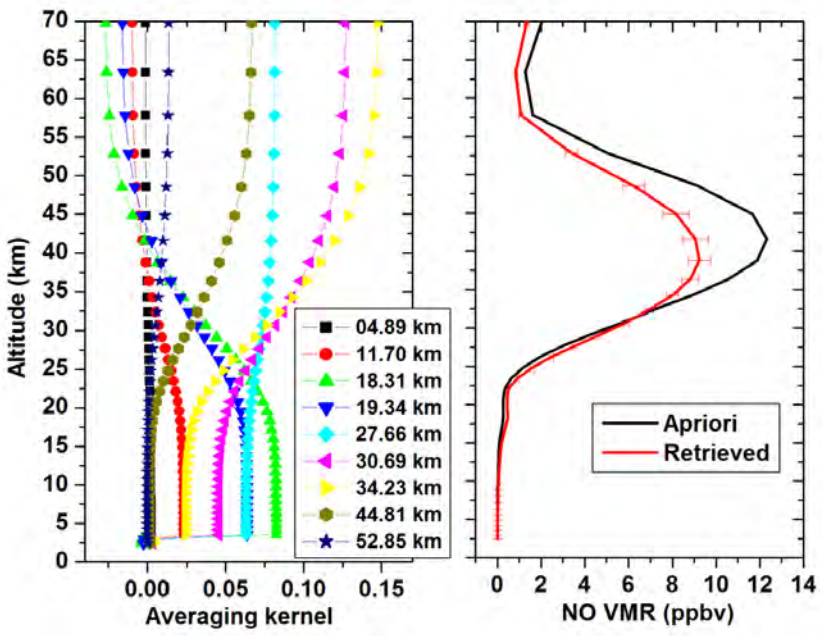

Figure 7.3: [Left panel] Averaging kernel of NO for selected heights and [Right panel] retrieved profile on 26 Novemeber 2009 at a SZA of 59.66^0.

7.2 Error analysis

The error analysis is based on the work of Rodgers (2000) [19], according to which the error in the retrieved profiles separates into three components; errors due to uncertainties in the input parameters applied in the inversion procedure, errors due to measurement noise, and errors due to the inherent finite vertical resolution of the observing system. The error for spectral base line (offset, channelling), ILS (linear modulation loss and constant phase error), LOS, temperature, spectroscopic data and spectral noise are evaluated.

The random and systematic errors of the retrieved NO and NO_2 are shown in Figs. 7.4-7.5. The percentage error of both gases are listed for some selected heights in Tables 7.2 and 7.3. The figures show the square-root of the variances of the spectral noise and individual model parameters contributions to the random error covariance matrix of both gas retrievals, as well as the combined random error. The structure in the

Table 7.2: summarization random error (%), at selected altitude. For NO_2 on 30 May, 2009 and NO on 26 Dec, 2009. Each row NO_2 at top and the bottom NO.

Altitude(km)	Baseline	ILS	LOS	Solar	Noise	Total stat.
2.45	38.24	0.150	0.076530	0.206	3.81	38.44
	22.95	2.940	0.053562	23.95	9.17	34.54
10.72	37.85	0.148	0.076500	00.20	3.79	38.05
	22.25	2.870	0.053558	23.59	9.03	33.66
17.12	35.59	0.141	0.076570	00.18	3.67	35.76
	18.60	2.470	0.053557	19.57	8.07	28.29
24.81	20.15	0.126	0.077010	00.06	2.80	20.35
	08.89	01.22	0.053557	08.36	4.34	13.01
32.37	04.60	0.169	0.077370	00.05	3.21	05.64
	00.66	0.260	0.053578	02.63	2.47	03.70
52.85	03.48	0.201	0.077540	00.11	3.93	05.27
	09.51	01.56	0.053674	12.73	8.02	17.87

error profiles shape reflects the effect of the propagation of the different errors in the retrieval process.

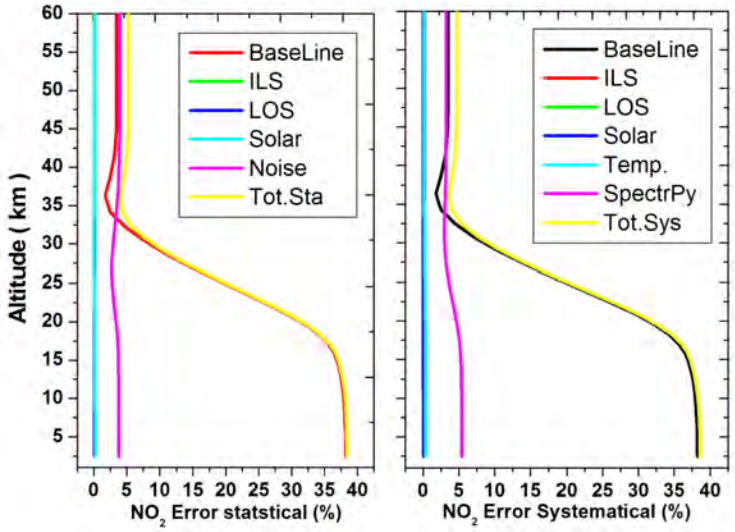

Figure 7.4: [Left panel] random (statstical) error and [Right panel] systematical error (%) for NO_2, on 30 May 2009.

The major sources of random uncertainties are the baseline and spectral noise error for NO_2. Specialy in the troposphere from ground upto 17.12 km baseline error dominates

Table 7.3: summarization systematical error (%), at selected altitude. For NO_2 on 30 May, 2009 and NO on 26 Nov, 2009. Each row NO_2 at top and the bottom NO.

Altitude(km)	Baseline	ILS	LOS	Solar	Temp	Spec.scoPy	Total syst.
2.45	38.24	0.150	0.008504	0.052	0.339	5.42	38.62
	22.95	2.940	0.005952	5.990	0.270	3.49	24.16
10.72	37.85	0.148	0.008505	0.050	0.338	5.37	38.23
	22.25	2.870	0.005950	5.850	0.260	3.43	23.43
17.12	35.59	0.141	0.008510	0.045	0.330	5.12	35.94
	18.60	2.470	0.005949	4.890	0.230	3.07	19.64
24.81	20.15	0.126	0.008557	0.016	0.260	3.60	20.47
	08.89	1.220	0.005950	2.090	0.180	2.25	09.84
32.37	04.60	0.169	0.008598	0.014	0.182	2.98	05.49
	00.66	0.260	0.005953	6.580	0.150	2.53	02.71
52.85	03.48	0.201	0.008616	0.027	0.145	3.21	04.74
	09.51	1.560	0.005963	3.180	0.110	3.86	10.86

over other sources of error such as an offset signal, channelling. This is mainly due to nonlinearity of the detector MCT because of its high sensetive. It is also the dominat factor for systematic uncertainity. The uncertainties coming from the spectral measurement noise are defined as a diagonal matrix consisting of the squared noise in the observed spectra. For systematic error spectroscopic line parameters is the secondary contributer as shown in Table 7.3 (less than 5.42%). The ILS, LOS, solar and temperature errors are very small. In general for this gas systematic error is larger than random error by small value.

Also clearly seen in Table 7.2 and Fig.(7.5) that dominant sources of random uncertainties for NO are solar, baseline and spectral noise error. The maximum error occur from the discrepancies between the angle under which the solar radiation enters the instrument and the actual solar elevation angle, which is applied in the retrieval. This may occur when the instruments aperture is not centred on the solar disk in during the measurement. In troposphere from ground upto 17.12 km solar error dominat accounting for 19.57% to 23.95% and but this error contributes less than 6% systematic

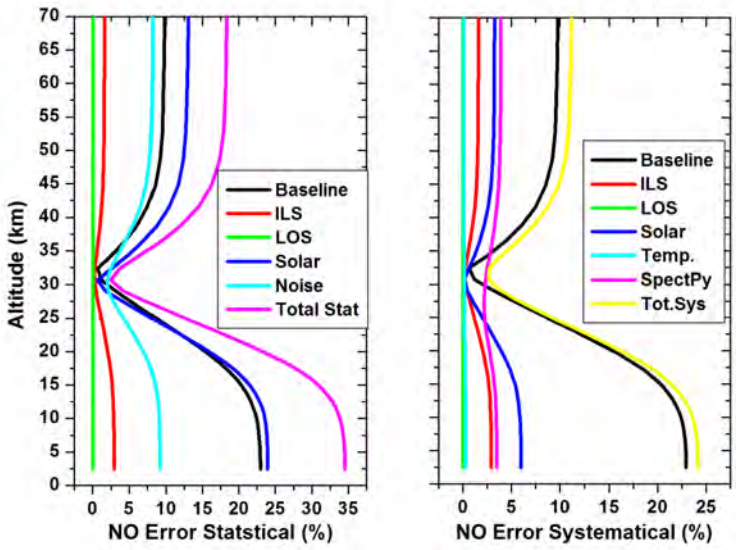

Figure 7.5: [Left panel] random (statstical) error and [Right panel] systematical error (%) for NO, on 26 Nov, 2009.

error. The uncertainties coming from the measurement noise have been determined in the same manner for NO_2 and found out to be less than 10% this error comes from the strongest absorber interfering gas of H_2O specially in troposphere region where as other sources of error is less than 3%. In general for this gas random error is larger than systematic error by 10%.

7.3 Vertical Profiles

One of the issues of this thesis is to retrieve vertical profile of NO_x members individually as NO and NO_2 over Addis Abeba at the high-altitude site in tropical region. The vertical profiles both trace gases form solar attenuated spectra measured by FTIR spectrometer is retrieved with three IDACC filter band, in microwindows that are given in Table 7.1. We have used slope regularization method for the retrieval of both target gas profiles while the signature of interfering species is calculated by simple scaling of

start profile. DOFs for both gas are about 1. As a result much of our focus is on the column amount rather than vertical profiles.

NO_2 retrieved and apriori profiles are shown in Fig.7.2, right panel. The retrived profile between 14 km and 32 km has a great slope that differs the apriori. The cause due to high interferences with CH_4, topography factor (Altitude, Tempreture) and unknown lines. The retrived profile has a maximum VMR of 2.76 ppbv at 34.23 km in stratosphere.

NO retrieved and apriori profiles are shown in Fig.7.3, right panel. The retrived profile between 9 km and 39 km has great variable slope. The cause due to high interferences with CO_2, topography factor and unknown lines. The retrived profile has maximum VMR of 9.247 ppbv at 38.77 km in stratosphere.

Time variation

On december 22, 2010 we have taken 5 measurments of NO_2 in 1Hr gap time beginning at 07:12 and ending at 11:12 GMT and on this day we also have 4 measurments of NO from 07:53 to 10:54 GMT. Fig. 7.6 shows the varition for different altitude in stratosphere.

The figure shows that the VMR of NO and NO_2 increases at morning due to the photolysis reaction that dissociate the night time reserviours of nitrogen oxides. When the sun is overhead the VMR of NO_2 decreases but NO increases because NO_2 molecules that produced in the morning photolysed by absorbing sun radiance into NO and O also the night time reserviours that completely gone to produce NO. For NO especially at 38 and 41 km the stepper is very fast than at 33 km which indicates that there is an additional sources that increases its production which is likely to be the photodissociation of the greenhouse nitrogen gas N_2O in the upper stratosphere. In

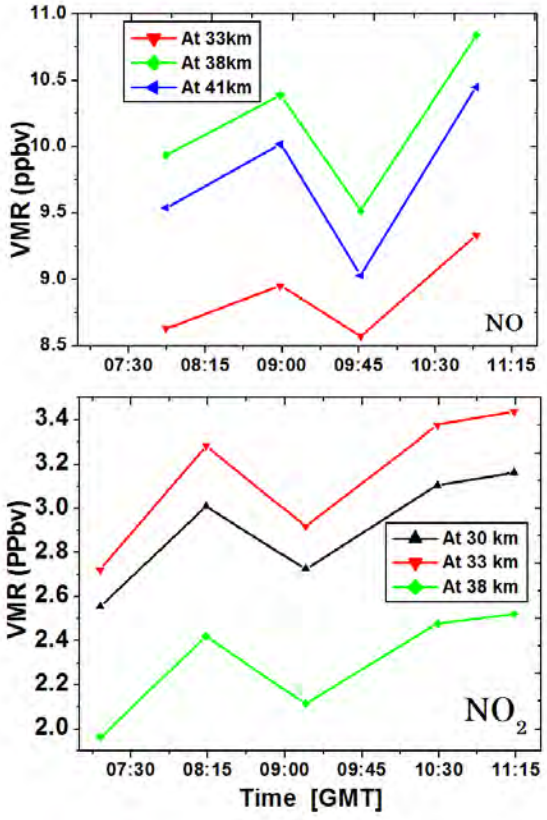

Figure 7.6: Hourly time variation in Stratosphere of NO [Upper panel] and NO_2 [lower panel] on 22 December, 2010.

this part of stratosphere, more energetic photons that comes from sun radiation dissociate 90% of N_2O There is also possibility for other source reaction like thermalization of N_2 with oxygen ion atom produced from dissociation of O_2 in upper stratosphere and mesosphere.

Vertical variation in near ground

Variation of NO and NO_2 concentration in the lower troposphere posses main cruicial environmental issue because these molecule controls the photochemistry processes of this layer of the atmosphere.

We have shown the vertical variation of these radical species near ground for measurement taken on 22 Dec, 2010, as shown in Fig. 7.7 in four panels for different time of

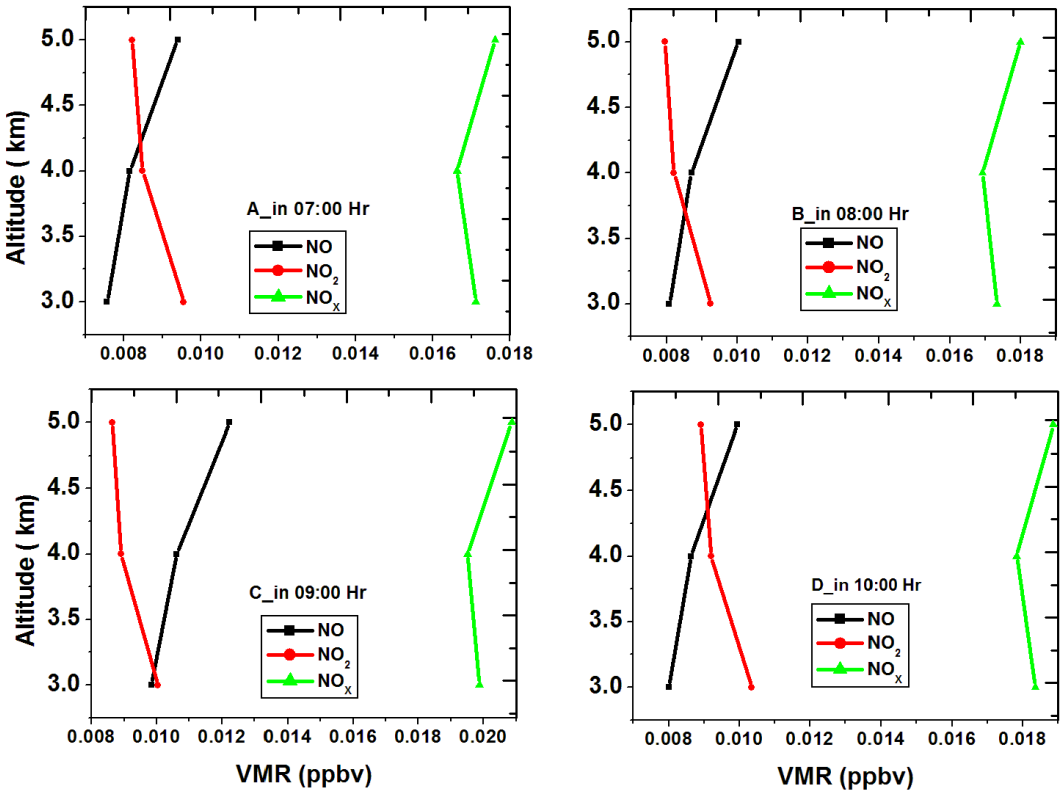

Figure 7.7: Vertical variation of for NO_x from ground upto 5 km on 22 Dec, 2010 in four different time.

the day (A-07:00, B-08:00, C-09:00 and D-10:00). We see from these graphs that all have source on ground but differ when the altitude increases. As shown in panel A of Fig. 7.7, NO_2 VMR exceeds that of NO because NO that is produced near the ground immediately changes into NO_2. This is in agreement with the condition that at this time also the wavelength sun light that dissociate NO_2 molecule did not reach at 3 km. At higher levels exceeding 3 km, NO_2 VMR decreases along with build up of NO. Subsequently, the two curves intersect at 4 km above which much of NO_2 photolyses into NO.

After an hour measurment as shown in panel, B-08:00 GMT the gap in VMRs of these

gases decreases at 3 km and also the intersection point is below 4 km due to the available wavelength of sun light to dissociate NO_2 below 4 km into nitric oxide and oxygen atom.

In panel C-09:00 GMT, the gap in VMRs of these gases becomes narrower at 3 km and also the intersection point is nearer to 3 km for the same reason as for panel B-08:00 GMT. Finally in panel D-10:00 GMT the same situation as in panel A-07:00 GMT. NO molecule that is produced by the previous condition can react other species like ozone in the atmosphere so taht NO_2 at 3 km and 5km increases and the intersection point is above 4 km.

Table 7.4: Summation of VMR NO and NO_2 as NO_x ppbv for 3, 4 and 5 km altitude near ground on 22 Dec, 2010 in different time.

Altitude	07:00GMT	08:00GMT	09:00GMT	10:00GMT
3	1.711E-2	1.7332E-2	1.9875E-2	1.8363E-2
4	1.6926E-2	1.6629E-2	1.9517E-2	1.7831E-2
5	1.8003E-2	1.7613E-2	2.0863E-2	1.8867E-2

Column amount

The partial column and the integrated columns of NO and NO_2 are shown in Fig. 7.8 based on a data taken on 30 May, 2009 measurment. These two graphs (left and right panels) show that the vertical distribution of the gases as well as the levels at which the highest concentration are found. Partial column amount at the left panel of Fig. 7.8 shows that the concentrations of the partial column of NO_2 exceeds that of NO at the ground in between 2.45 km and 2.94 km likely due to biomass burning.

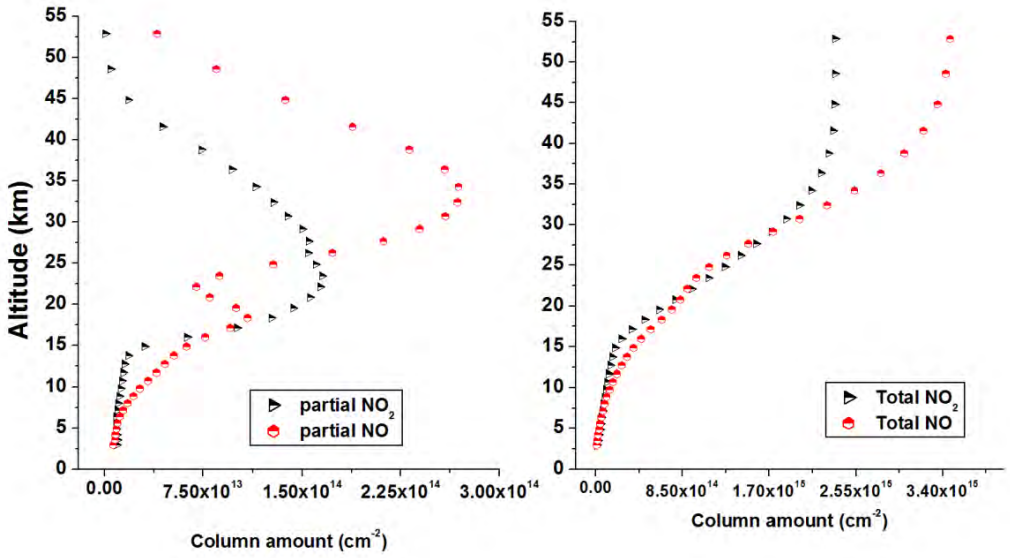

Figure 7.8: column amount [left] partial and [right] total for NO and NO_2 on 30 May, 2009.

7.4 Time series of NO_x column amount

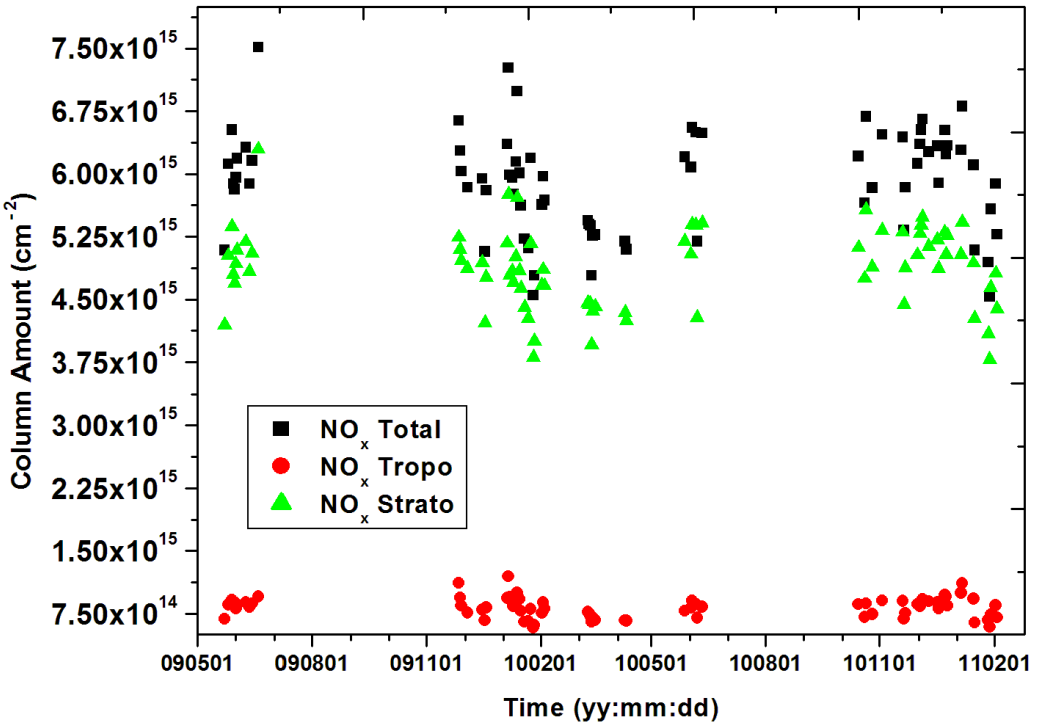

Figure 7.9: Time series of the total column NO_x as a whole upto 85 km (rectangle black colour), stratosphere (triangle green colour) and troposphere (cirlcle red colour).

We have 75 days of measurment data for both gases on the same day so we have analysed the time series of the total, stratosphere and troposphere column amounts of NO_x ($NO + NO_2$) from May 2009 to February 2011 and the time series for stratosphere and troposphere column amounts of NO_x on monthly and seasonal time scales for 2010. The number of measurements with in this period is due to unaffordable natural phenomena of the rainy season (from June-September 2009 /10), unexpected cloud cover over Addis Ababa which severely limited the observing capability of our FTS.

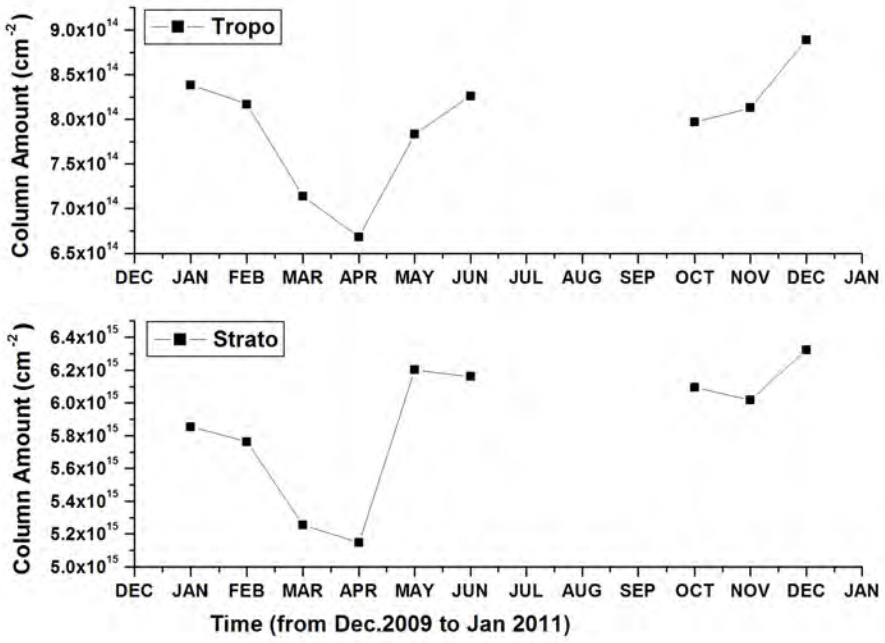

Figure 7.10: Time series of monthly mean column amount of NO_x in stratosphere(lower panel) and troposphere(upper panel) of 2010 months.

Fig. 7.10 shows mean monthly NO_x VMR for the period January 2010 to January 2011. There is a distinct seasonal variation in NO_x except for data gap during the rainy months from July to September. The seasonal variation seems to follow position of the sun viz-viz SZA. This seasonal variation is well characterized by the sum of spring, winter, summer and autumn months in Fig. 7.11.

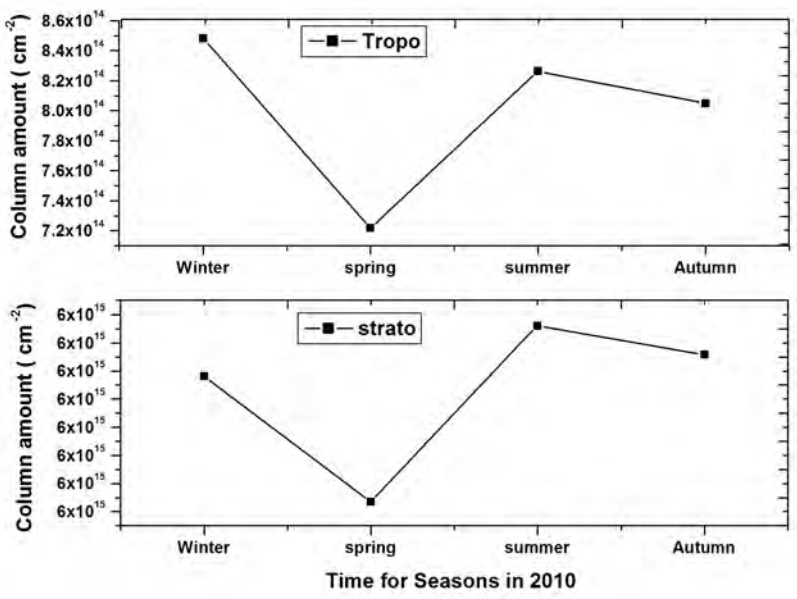

Figure 7.11: Time series in seasonly variation of NO_x column amount in stratosphere(lower panel) and troposphere(upper panel) in 2010.

7.5 Validation of FTIR NO_2 with OMI Level 3 data

The OMI instrument is a nadir-viewing imaging spectrometer measuring direct and atmosphere backscattered sunlight in the UV/VIS range from 270 to 500 nm (Levelt et al., 2006). It was launched onboard the Aura satellite on 15 July 2004, and put into a Sun-synchronous, polar orbit at an altitude of about 705 km with an equator crossing time between 13:40 and 13:50 LST. OMI employs two two-dimensional CCD detectors that record the (ir)radiance spectrum in UV (270-310nm and 310-365 nm) and VIS (365-500 nm) regions, respectively. Over the OMI FOV (114^0), 60 discrete viewing angles are distributed perpendicular to the flight direction. The FOV corresponds to a 2600-km-wide spatial swath on the Earths surface, achieving daily global measurements. Nadir spatial resolution ranges from 13×24 to $24 \times 48 km^2$, depending on the operation mode [25].

The OMI data products are available at four processing levels: Level 0, Level 1B, Level

2, and Level 3. For Level 0, Level 1B, and Level 2 products contain orbital swath data, where as Level 3 products contain global data that are composited over time (daily or monthly) or over space for small equal angle (latitude×longitude) grids covering the whole globe. Level 3 Products based on each Level 2 product file contains data from a single orbit. For each Level 2 product there are 14 files per day. OMI Level 3 daily global products are produced by using best pixel data over small equal angle grids($0.25^0 \times 0.25^0$), ($0.5^0 \times 0.5^0$) or ($1^0 \times 1^0$) covering the whole globe [26]. For the purpose of validation of our FTIR NO_2 data OMI Level 3 data for 92 coincident days of measurement of daily mean column amount in a latitude-longitude range of 8.5-9.0 degree N and 38-39 degree E over Addis Ababa.

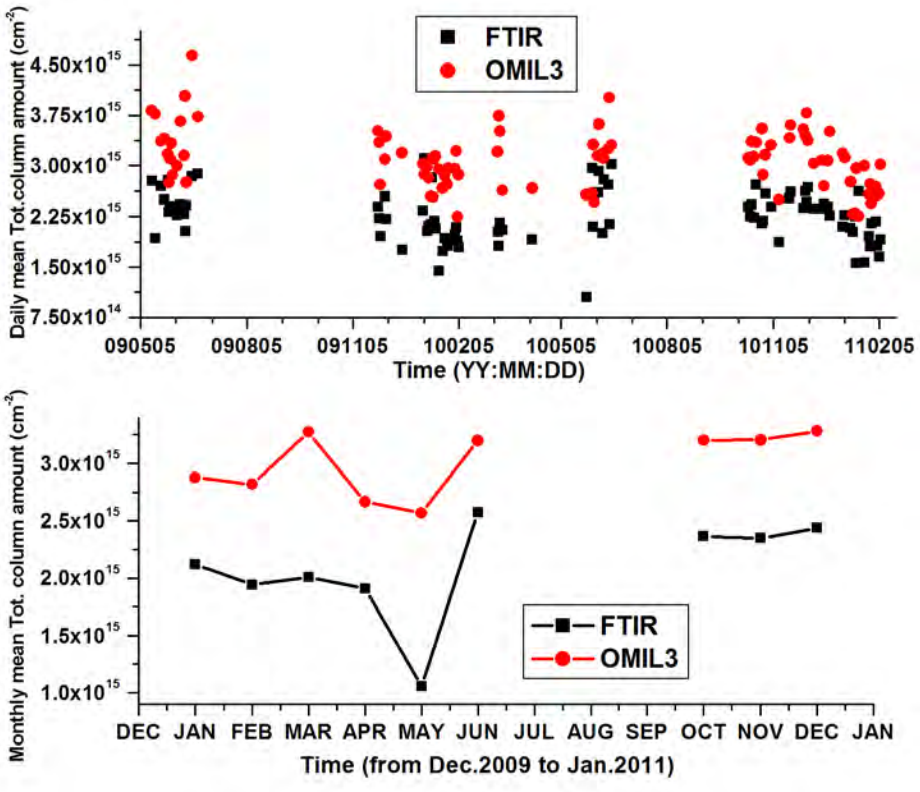

Figure 7.12: FTIR and OMIL3 NO_2,Time series in daily mean total column amount (upper panel) and monthly mean total column amount in 2010 (lower panel).

Fig. 7.12 shows the column amount of NO_2 from OMI (red) and FTIR (black) for daily (top panel) and monthly mean (bottom). The OMI NO_2 total column is higher than that of FTIR for both daily and monthly mean. One of the possible explanations for this difference is that OMI measurements are carried out for the full 24-Hr period as compared to day time measurement which for this specific case limited to 9 am to 4 pm local time. This is because FTIR does solar absorption measurement. As a result, FTIR measurement times does not include time of the day at which NO_2 attains its peak which are early morning and late afternoon. This difference is also evident from scatter plot given in Fig. 7.13 which shows low bias in FTIR NO_2 against OMI NO_2.

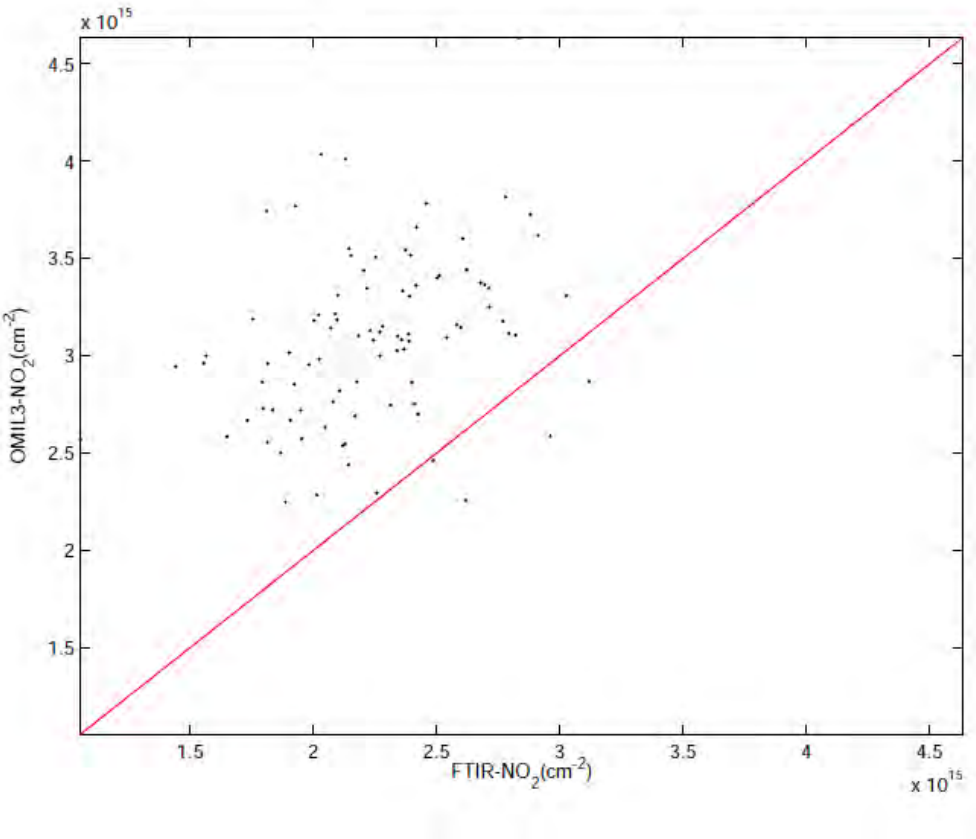

Figure 7.13: FTIR and OMIL3 NO_2, daily mean total column amount scatter plot.

Chapter 8

Conclusion

Ground-based FTIR spectroscopy is a very useful technique to derive total column abundances and low-resolution vertical profiles of many important trace gases in the atmosphere. The technique is being used at many stations worldwide, mostly in the frame of IDACC, but rarely at high-altitude tropical stations. Up to now, there are no regular high resolution FTIR measurements in the tropics. The instrument was found to be well aligned during the whole gas cell measurement period of a month. The instrumental line shape fit to HBr gas cell measurment in our site for 2500.00-2500.12cm^{-1} wavenumber region shows a very good fitting with the residual $< 1\%$, in between the measured and simulated transmission spectra.

The results of spectral fit to determine NO and NO_2 gives residual in all microwindows which are less than 1% for NO and 0.1% for NO_2 and also average signal noise ratio in the spectral regions used for NO and NO_2 are 352.62 and 2863.92 respectively. The quality of NO and NO_2 vertical profile retrival from ground-based FTIR observation was evaluted using a full error budget, vertical resolution and DOF. The mean column amount of NO_2 is compared to OMI NO_2 column amount despite differences in what the two columns represent. The comparison has shown that the differences between OMI daily and monthly means lie on the right side thereby revealing OMI NO_2 exceeds FTIR NO_2 column amounts. Both NO and NO_2 as well as NO_x time series of VMR

profiles and column amounts (partial and total) exhibit daily and seasonal variation which are consistent with physics of transport and photochemistry. The partitioning of nitrogen radical between NO and NO_2 at different altitude levels (surface, troposphere and stratosphere) as well as on temporal scales is consistent with photochemistry of NO_x and its precursors.

In summary, the retrieved NO and NO_2 profiles and column amounts from FTIR observation over Addis Ababa are very vital for studies related with long term atmospheric composition changes and air pollution. However, further measurements, validation of NO_x should be pursued while as the same time studies on air pollution from perspective NO_x should also pursued along with other diagonistics.

Bibliography

[1]. David G.Andrews, An Introduction to Atmospheric Physics. (Cambridge University Press, New York, 2010).

[2]. J.H.Seinfeld and S.N.Pandis, Atmospheric chemistry and physics. (John Wiley and Sons., New Jersey, USA, 2006).

[3]. K.Mohanakumar, Stratosphere Troposphere Interactions. (Springer Science + Business Media B.V., Cochin,India, 2008).

[4] Sebastian Trick,(2004). Formation of Nitrous Acid on Urban Surfaces: a physical-chemical perspective. Ph.D Dissertation, Combined Faculties for the Natural Science and for Mathematics of the Ruperto Carola University Heidelberg, Germany.

[5]. Logan, (1983). Nitrogen Oxides in the Troposphere, Journal of Geophysical research. 88, 10,785-10,807.

[6]. R.F.Fouett and J.L. Hatfield, Nitrogen in the Environment: Sources, Problems, and Management. (Elsevier B.V., Amsterdam, Netherlands, 2001).

[7]. Bradshaw et al,(2000). Observed distribution of Nitrogen oxides, REVIEWS OF GEOPHYSICS. 38,61-116 Amer.Geo.Un.

[8]. U.Schumann and H.Huntrieser, (2007): The global lightning-induced nitrogen oxides source, Atmos.Chem.Phys., 7, 38233907.

[9]. Finnlayson-Pitts,B.J. and Pitts,J.N, Chemistry of the upper and Lower Atmosphere. (Academic Press, California, 2000).

[10]. Celarier,E.A., et al.Validation of Ozone Monitoring Instrument nitrogen dioxide columns. J.GEOPHYS. RES., 113, D15S15, (2008).

[11]. K.N.Liou, An Introduction to Atmospheric Radiation. (Academic Press., San

Diego, USA, 2002).

[12]. Charlie Zender. (2008), Notes for Students of ESS 236: Radiative Transfer in the Earth System. Department of Earth System Science, University of California, Irvine.

[13] Brain C.Smith, Quantitative Spectroscopy: Theory and Practice (Academic Press., San Diego, California, USA, 2002).

[14]. J.Michael Hollas, Modern Spectroscopy $4^{th}Ed$ (John Wiley and Sons Ltd, Chichester, England, 2004).

[15]. W.Demtrder, An Introduction Atomic, Molecular and Quantum-Physics. (Springer-Verlag, Berlin Heidelberg, Germany, 2006).

[16]. User Manual of IFS125HR FTIR spectrometer.

[17]. Milikessa, G.(2010). Stratospheric AEROSOL climatology from SAGE II and observation of its driver,CARBONYL SULFIDE over Equatorial Africa. MSc. thesis, Physics Department, Addis Ababa university.

[18]. Wiacek,A., et al,(2007), Ground-Based Solar Absorption FTIR Spectroscopy: Characterization of Retrievals and First Results from a Novel Optical Desighn Instrument at a new NDACC Complementary Station. Journal of Atmospheric and Oceanic Tech. 24, 432-448.

[19]. C.D.Rodgers, Inverse methods for Atmospheric sounding:Theory and practice (World scientific, Singapore. 2004).

[20]. Gang Li,(2003), Fourier Transform Spectroscopy of Selected Transient Species. Ph.D Dissertation, Department Chemistry, University of Waterloo,Ontario, Canada.

[21]. Siegfried Wartewig, IR and Raman Spectroscopy:Fundamental Processing.(WILEY-VCH Verlag GmbH and Co.KGaA,Weinheim, Germany, 2003).

[22]. Hase, F.,(2000). Inversion von spurengasprofilen FTIR-Messungen in Absorption, Dissertation, genehmigt von der Facultat fur physik der Universitat Karlsruhe(TH).

[23]. Anna Katinka Petersen, (2009). Atmospheric Trace Gas Measurements in the Tropics, Ph.D Dissertation, Fachbereich fur, Physik und Elektrotechnik, University of Bremen,Bremen, Germany.

[24]. M. Schneider et al,(2005). Measured and modeled five-year time series of subtropical trace gas profiles, Atmos.Chem.Phys., 5, 153 -167.

[25] Boersma,Folkert (2005). Satellite observations of tropospheric nitrogen dioxide:retrieval, interpretation, and modelling, Eindhoven: Technische Universiteit Eindhoven, The M.C. Escher Company B.V. Baarn-Holland.

[26] J.P.Burrows, U.Platt and P.Borrell. The Remote Sensing of Tropospheric Composition from Space: Data Quality and Validation of Satellite Measurements of Tropospheric Composition. (Springer Verlag, Heidelberg, Germany,2011).

Declaration

This thesis is my original work, has not been presented for a degree in any other University and that all the sources of material used for the thesis have been dully acknowledged.

Name: FRIEWELEGA GELETA HUNDE

Signature:_____

Place and time of submission: Addis Ababa University, June 2011

This thesis has been submitted for examination with my approval as University advisor.

Name: Dr.GIZAW MENGISTU

Signature:_____